Redshift dependence of soft X-ray quasar spectra

N. Schartel¹, R. Walter^{1,2}, H.H. Fink¹, and J. Trümper¹

¹ Max-Planck-Institut für extraterrestrische Physik, D-85740 Garching bei München, Germany

Received 18 November 1994 / Accepted 8 July 1995

Abstract. The analysis of the X-ray spectra of a sample of 102 X-ray bright quasars observed with ROSAT during the all-sky survey confirmed for the soft (0.1 - 2.4)keV energy range that the power law photon indices of radio-loud and radio-quiet quasars differ significantly from each other: $\langle \Gamma \rangle_{rl} = 2.23 \pm 0.07$; $\langle \Gamma \rangle_{rq} = 2.54 \pm 0.04$. These mean indices are found to be significantly steeper than those determined for the harder (0.3 - 3.5)keV energy band of the *Einstein Observatory/IPC* and the medium energy (2 - 10...20)keV bands of the EXOSAT/ME and *Gingal/LAC* experiments for identical subsets of quasars. The comparison yielded a tendency of the harder the energy range covered by the experiment the flatter the average spectral indices.

All but one of the 55 radio-quiet quasars in the present ROSAT sample cover a very limited redshift range (z < 0.5). On the other hand, the 47 radio-loud quasars of the sample have redshifts up to z = 2.5. For this subset we established a relation between the mean photon index in ROSAT's soft energy band and the redshift. This relation shows a remarkable drop of the spectral slope from $<\Gamma>\sim 2.2$ for nearby quasars to $<\Gamma>\sim 1.5$ for distant objects. This flattening of the mean quasar spectrum with increasing redshift may partly be caused by selection effects. A quantitative interpretation of the relation is, however, achieved by assuming a two-component continuum for the intrinsic mean quasar spectrum consisting of a medium energy power law spectrum and a steep soft excess component.

As far as the spectral properties at very soft X-ray energies are concerned, radio-loud and radio-quiet quasars are indistinguishable. Normalized to the same soft excess component, the power law continua of radio-loud and radio-quiet quasar cross over at about 0.6 keV. Beyond that photon energy the radio-loud quasars are appreciably X-ray brighter and spectrally flatter than their radio-quiet counterparts. The only difference between both species seems to be a difference in the medium energy spectral index.

Key words: X-ray: galaxies – quasars: general

1. Introduction

Already in the early years of X-ray astronomy quasars as objects at cosmological distances were subjects of intensive X-ray studies (e.g. 3C 273: Bowyer et al., 1970). Up to these days, the X-ray spectra of individual nearby and distant quasars are measured (e.g. Kolman et al., 1993; Elvis et al., 1994; Yaqoob et al., 1994; Serlemitsos et al., 1994; Wilkes et al., 1992a; Fink & Briel, 1993) to elucidate the role of the high energetic processes producing X-rays relative to the overall energy distribution of the quasar emission. In the X-ray energy band (0.3 - 3.5)keV of the IPC detector onboard the Einstein Observatory the study of smaller samples of quasars (Zamorani et al., 1981; Elvis, Wilkes, and Tananbaum, 1985; Elvis et al., 1986) and of a larger sample of 33 quasars (z < 1.0) (Wilkes & Elvis, 1987; Canizares & White, 1989; Worrall, 1989) yielded a wide spread in the power law index in contrast to the tighter index distribution of medium energy spectra in the (2 - 10)keV band found for lower luminous Active Galactic Nuclei (AGN) (Mushotzky, 1984; Turner & Pounds, 1989, Nandra & Pounds, 1994). These studies further revealed the dichotomic character of the X-ray spectra of quasars with respect to their radio properties. Radio-loud quasars show flatter spectra in the Einstein band than radio-quiet QSOs, and they are X-ray brighter at 2 keV than their radio-quiet counterparts. The X-ray spectra of 31 quasars were measured with EXOSAT (Lawson et al., 1992) in the (2-10)keV band. The medium energy spectra between 2 keV and 20 keV of further 13 quasars could be established with Ginga (Williams et al., 1992). They confirmed the earlier finding that the slopes of the X-ray spectra of radio-loud and radio-quiet quasars are different also at higher photon energies. Furthermore, the analysis of quasar spectra obtained with the LE and ME detectors onboard of EXOSAT revealed that at least half of the quasars studied showed indications of a soft flux excess in their spectra below 1 keV (Comastri et al., 1992; Saxton et al., 1993). Such soft X-ray excesses have firstly been found in the X-ray spectra of Seyfert 1 galaxies by Arnaud et al. (1985) and Singh et al. (1985). The measurement of soft Xray spectra with the PSPC detector of the X-ray telescope of ROSAT confirmed that a large fraction of X-ray bright Seyfert

² Observatoire de Genève, Chemin de Maillettes 51, CH-1290 Sauverny, Switzerland

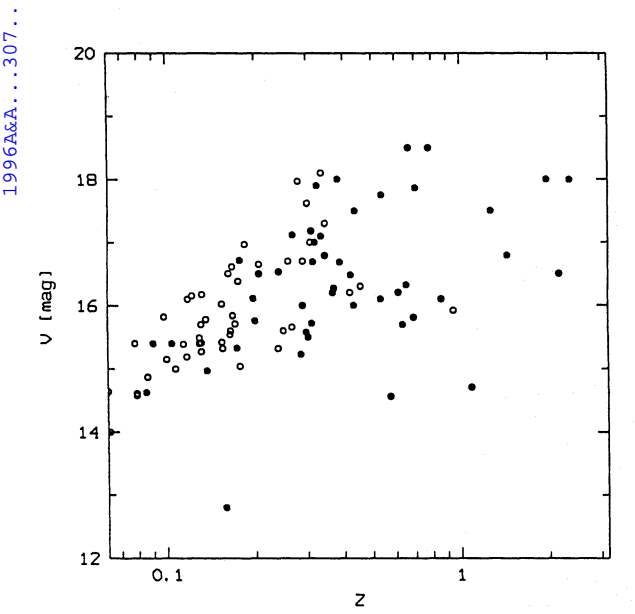


Fig. 1. The sample. Visual magnitude vs. redshift of the sample quasars. Open circles: radio-quiet quasars; filled circles: radio-loud quasars.

1 galaxies shows steep spectra indicating an excess flux at low photon energies over the extrapolation of the medium energy power law with a mean index of $<\Gamma>=1.8....1.9$ (Walter & Fink, 1993). Studying the spectra of quasars measured with the Einstein/IPC Schwartz, Qian, and Tucker (1990) noticed that two-component model spectra consisting of a medium energy power law and thermal bremsstrahlung at soft photon energies give equally good fits that a simple power law. The X-ray spectral study of small samples of quasars extracted from pointed observations with ROSAT confirms the steepness of the soft X-ray spectra for quasars (Laor et al., 1994; Fiore et al., 1994).

In this paper we present the soft X-ray spectral properties of a larger sample of radio-loud and radio-quiet X-ray bright quasars with redshifts up to $z \sim 2.5$ as measured with the X-ray telescope onboard ROSAT during the all-sky survey. In Sect. 2, we define the sample of quasars and compile some of their spectral properties. The analysis of the quasars' X-ray data is described in the following section, in which we, additionally, develop the statistical tools needed to estimate the spectral parameters for weak X-ray sources. In Sect. 4, we present the results: firstly, we determine the sample means of the power law indices of the ROSAT spectra of radio-loud and radio-quiet quasars, respectively, and compare them with those derived from other satellite experiments for identical subsets of the present quasar sample. Secondly, a relation between the redshift of the sample members and their soft X-ray spectral indices is established. After discussing the influence of possible selection effects on this relation, we present an interpretation of the redshift relation based on the assumption that the mean intrinsic quasar spectrum shows a soft X-ray excess. Finally, we discuss the distinctions between radio-loud and radio-quiet quasars as follow from the present study. In Sect. 5, a summary and conclusions are given.

2. The data

2.1. The sample

During the all-sky survey performed with the ROSAT satellite observatory (Trümper, 1983) in 1990 about 60,000 X-ray sources were detected with a likelihood of more than 10 (Voges, 1992). We correlated the sky positions of these survey Xray sources, as derived by the Standard Processing and Analysis Software System (SASS; Voges et al., 1992), with those of the optically selected AGN listed in the Véron-Cetty & Véron catalogue (1991). A coincidence between both source lists was stated, if the celestial position of the X-ray centroid of a survey source deviates less than 50 arcsec from the well defined optical position of the AGN. The 1σ error of the position of an average survey source is 20 arcsec (Voges, 1992). According to the distribution of deviations of all coincidences, the limiting 50 arcsec radius corresponds to a fraction of misidentification of less than 1% (Schartel, 1994). The extracted list of X-ray/optical coincidences contained 1016 AGN. For the present study we selected those AGN which were assigned as QSOs in the Véron-Cetty & Véron catalogue ($M_V < -23.0$). To enable the estimation of spectral parameters we dropped in a second selection all sources, for which the SASS processing of the ROSAT data extracted less than 80 PSPC counts for the survey observation. This yielded a list of 104 QSOs from which two further sources had to be excluded: 3C 345 was removed because of its classification as OVV (Angel & Stockman, 1980) and KUV 1821+643 was excluded because it coincides positionally almost with the white dwarf K1-16; due to the limited spatial resolution during the survey the QSO and the white dwarf cannot be resolved as separate X-ray sources (Ulrich et al., 1992). The final list of 102 quasars with more than 80 PSPC SASS-counts is given in Table 1.

2.2. Radio, optical, and previously published X-ray data

Quasi-stellar objects show an enormous range of radio power. To characterize the radio emission of a quasar relative to its optical flux a radio-loudness parameter is used which is defined as the K-corrected ratio of radio (5 GHz) to optical (B band) fluxes (Sramek & Weedman, 1980)

$$\alpha_{RO} = \frac{1}{5.38} \log \left(\frac{S_{5GHz}}{S_{2500\text{Å}}} \right) = \frac{1}{5.38} \left[\left(\log S_{5GHz} + 0.7 \log(z+1) \right) - \left(23.0 - 19.76 - 0.4 \text{V} + 1.0 \log(z+1) \right) \right]$$

Here, the spectral fluxes have to be given in units of Jy. V is the quasar's visible magnitude. Using this radio-loudness parameter it has been shown that optically selected QSOs can be consistently separated into two distinct classes: radio-loud and radio-quiet; the distribution of α_{RO} revealed to be bimodial at a high level of confidence (PG sample: Kellerman et al., 1989; EMSS AGN sample: Della Ceca et al., 1994). For the EMSS AGN sample this distribution shows a gap for $0.25 \le \alpha_{RO} \le 0.35$ (Della Ceca et al., 1994). Following this criterion we regard all

Table 1. The sample, ordered by redshift and grouped to redshift bins

	1 /	J						
No.	Object	Position		z	V	M_V	$\log \lambda L_{\lambda}^{(a)}$	α_{RO}
		RA	Dec		[mag]	[mag]	[erg/s]	
	1 6771 500	00.41.06.0	a) Radio-q			00.6	44.00	0.074
1	MKN 509	20 41 26.2	-10 54 17	0.035	13.12	-23.6	44.88	-0.074
2	ESO 141-G55	19 16 57.0	-58 45 52	0.037	13.64	-23.1	44.69	0.170
3	4U 0241+61	2 41 00.6	62 15 27	0.044	12.19	-24.9	46.71	0.172
4	F9	1 21 51.2	-59 03 59	0.045	13.25	-23.9	44.98	0.020
5	MKN 926	23 02 07.2	-8 57 20	0.047	13.76	-23.5	44.82	0.039
6	Q 0959-079	9 59 30.9	-7 55 15	0.055	14.64	-23.0	44.65	
7	F 1116	3 49 54.0	-40 37 30	0.058	14.67	-23.0	44.60	0.020
8	IZw 1	0 50 57.8	12 25 20	0.061	14.03	-23.8	44.97	-0.030
9	II Zw 136	21 30 01.2	9 55 01	0.063	14.64	-23.3	44.76	-0.018
10	PG 0844+349	8 44 33.9	34 56 09	0.064	14.00	-23.9	44.98	
11	MKN 584	1 57 51.1	2 25 40	0.078	15.40	-23.0	44.62	0.079
12	MKN 478	14 40 04.6	35 39 07	0.079	14.58	-23.8	44.90	-0.078
13	VII Zw 118	7 02 24.1	64 40 39	0.079	14.61	-23.8	44.97	0.057
14	MKN 1383	14 26 33.8	1 30 27	0.086	14.87	-23.7	44.89	-0.057
15	PG 1404+226	14 04 02.8	22 37 59	0.098	15.82	-23.1	44.63	0.013
16	PG 0804+761	8 04 35.4	76 11 32	0.100	15.15	-23.7 -23.9	44.90 44.94	0.019
17	IR 1334+2438	13 34 57.4	24 38 18	0.107	15.			
18	MKN 877	16 17 56.5	17 31 35	0.114	15.39	-23.7	44.92	-0.019
19	TON S210	1 19 30.2	-28 36 34 48 25 56	0.117	15.19	-24.0	44.99 44.63	
20	PG 0906+48	9 06 45.3		0.118	16.10	-23.1 -23.1		
21	MKN 106	9 16 18.6	55 34 20	0.122	16.15 15.40		44.64	0.093
22	PG 1416-129	14 16 21.3	-12 56 58	0.129	15.49	-24.0 -23.9	45.09 44.97	0.093
23	MKN 876	16 13 36.2	65 50 37	0.129	15.49	-23.9 -24.1	45.05	0.044
24	MKN 813	14 25 05.7 8 38 32.0	10 03 17 77 03 59	0.131	15.7	-24.1 -23.7	44.87	
25	VII Zw 244		26 11 46	0.131	15.41	-23.7	45.03	0.112
26	TON 256	16 12 08.7 16 26 51.5	55 29 05	0.131	16.17	-23.2	44.67	0.112
27 28	PG 1626+554 KAZ 102	18 03 37.4	67 37 54	0.132	15.78	-23.2	44.93	
28 29	PG 1115+407	11 15 46.2	40 42 14	0.154	16.02	-23.7	44.87	
30	PG 0052+251	0 52 11.1	25 09 24	0.154	15.42	-24.3	45.16	-0.018
31	PG 1307+085	13 07 16.2	8 35 47	0.154	15.32	-24.5	45.20	-0.016
32	Q 0056-363	0 56 15.8	-36 22 17	0.162	16.5	-23.4	44.75	
33	PG 1402+261	14 02 58.8	26 09 59	0.164	15.54	-24.4	45.14	-0.009
34	GQ Com	12 02 08.9	28 10 54	0.165	15.60	-24.3	45.11	-0.004
35	PG 1048+342	10 48 56.1	34 15 23	0.167	16.61	-23.4	44.75	0.001
36	PG 1322+659	13 22 10.0	65 57 22	0.168	15.84	-24.1	45.04	
37	PHL 909	0 54 31.9	14 29 59	0.171	15.71	-24.3	45.16	
38	V 396 Her	17 20 37.7	24 39 06	0.175	16.38	-23.7	44.92	
39	PG 1116+215	11 16 30.1	21 35 43	0.177	15.04	-25.0	45.38	0.042
40	B 340	13 04 48.0	34 40 24	0.184	16.97	-23.2	44.66	
41	PG 0947+396	9 47 44.8	39 40 54	0.206	16.65	-23.8	44.91	
42	PG 0953+415	9 53 48.3	41 29 58	0.239	15.32	-25.5	45.58	0.029
43	US 1329	8 33 33.9	44 36 29	0.249	15.6	-25.3	45.53	
44	US 1107	9 52 30.4	45 46 31	0.259	16.7	-24.3	45.10	
45	PG 1444+407	14 44 50.3	40 47 40	0.267	15.66	-25.4	45.54	
46	AB 125	13 04 03.9	34 17 37	0.279	17.97	-23.2	44.66	
47	Q 0530-379	5 30 48.6	-37 55 26	0.290	16.7	-24.6	45.25	
48	TON 83	12 31 13.7	31 17 42	0.290	16.	-25.3	45.50	
49	В 337	13 05 29.4	35 17 49	0.300	17.62	-23.8	44.90	
50	CBS 56	12 14 50.5	31 13 24	0.307	17.	-24.5	45.19	
51	PC 1014+4717	10 14 25.9	47 17 27	0.335	18.1	-23.6	44.82	
52	Q 1214+0826	12 14 43.0	8 26 21	0.345	17.3	-24.4	45.15	
53	Q 1230+0947	12 30 53.6	9 47 55	0.420	16.2	-26.0	45.79	
54	US 737	9 31 50.4	43 44 36	0.456	16.3	-26.1	45.82	
55	PG 1407+265	14 07 07.7	26 32 30	0.944	15.92	-28.3	46.70	0.175
	FG 1407+203	1 T U I U I . I	20 32 30	0.277			41 NI A	

 $^{{\}small \circledcirc} \ European \ Southern \ Observatory \ \bullet \ Provided \ by \ the \ NASA \ Astrophysics \ Data \ System$

Table 1. (continued)

No.	Object		1 1 7.30.00	z	V	M_V	$-\log \lambda L^{**}$	α_{RO}
		RA	(1950.0) Dec	~	[mag]	[mag]	$\frac{\log \lambda L_{\lambda}^{(a)}}{[erg/s]}$	α_{RO}
			b) Radio-	loud Ona		[mag]	[~, 9/ 0]	·
56	PG 1211+143	12 11 44.8	14 19 53	0.085	14.63	-23.9	44.97	0.333
57	III Zw 2	0 07 56.7	10 41 47	0.090	15.40	-23.3	44.79	0.470
58	4C 74.26	20 43 13.0	74 57 08	0.104	15.4	-23.5	44.97	0.447
59	PKS 0558-540	5 58 34.6	-50 26 55	0.137	14.97	-24.5	45.25	0.338
60	3C 273	12 26 33.2	2 19 43	0.158	12.8	-27.0	46.19	0.650
61	PKS 2349-01	23 49 22.3	-1 25 54	0.173	15.33	-24.7	45.30	0.504
62	B2 1028+31	10 28 09.8	31 18 21	0.177	16.71	-23.4	44.75	0.497
63	PKS 1020-103	10 20 04.1	-10 22 34	0.197	16.11	-24.2	45.13	0.514
64	PKS 0837-12	8 37 27.9	-12 03 54	0.200	15.76	-24.7	45.35	0.542
65	B2 1721+34	17 21 32.0	34 20 42	0.206	16.5	-24.0	45.01	0.626
66	PKS 1217+02	12 17 38.3	2 20 21	0.240	16.53	-24.3	45.11	0.560
67	B2 1223+25	12 23 09.1	25 15 12	0.268	17.12	-24.0	44.99	0.498
68	PKS 1302-102	13 02 55.8	-10 17 17	0.286	15.23	-26.0	45.82	0.543
69	B2 1128+31	11 28 30.3	31 30 40	0.289	16.0	-25.3	45.52	0.464
70	B2 2201+31A	22 01 01.4	31 31 06	0.298	15.58	-25.8	45.87	0.617
71	4C 73.18	19 28 49.4	73 51 45	0.302	15.5	-25.9	45.87	0.640
72	B2 1351+26	13 51 18.0	26 46 32	0.310	17.18	-24.2	45.10	0.463
73	3C 249.1	11 00 27.4	77 15 08	0.311	15.72	-25.8	45.73	0.539
74	PKS 1451-375	14 51 18.2	-37 35 23	0.314	16.69	-24.8	45.39	0.681
75	4C 69.18	15 03 44.9	69 07 46	0.318	17.0	-24.5	45.21	0.535
76	PKS 2227-399	22 27 45.0	-39 58 17	0.323	17.9	-23.7	44.86	0.723
77	LB 2136	11 50 48.0	49 47 50	0.334	17.10	-24.6	45.23	0.671
78	PKS 1049-09	10 48 59.4	-9 02 13	0.345	16.79	-24.9	45.38	0.607
79	3C 48.0	1 34 49.8	32 54 20	0.367	16.20	-25.7	45.72	0.730
80	B2 1512+37	15 12 46.8	37 01 55	0.370	16.27	-25.6	45.62	0.549
81	PKS 1200-051	12 00 00.4	-5 11 20	0.381	18.0	-24.0	45.01	0.665
82	B2 1208+32A	12 08 05.4	32 13 48	0.388	16.68	-25.3	45.50	0.436
83	4C 61.20	10 49 22.4	61 41 18	0.422	16.48	-25.8	45.70	0.536
84	4C 09.72	23 08 46.5	9 51 57	0.432	16.00	-26.3	45.95	0.466
85	PKS 1222+21	12 22 23.6	21 39 24	0.435	17.50	-24.8	45.32	0.667
86	PKS 0454-22	4 54 02.2	-22 03 56	0.534	16.10	-26.7	46.10	0.575
87	3C 279	12 53 35.8	-5 31 08	0.536	17.75	-25.1	45.44	0.927
88	PKS 0405-12	4 05 27.5	-12 19 32	0.574	14.57	-28.4	46.79	0.525
89	4C 41.21	10 07 26.1	41 47 24	0.613	16.2	-27.0	46.18	0.562
90	MC 1104+167	11 04 36.7	16 44 17	0.634	15.70	-27.6	46.43	0.514
91	3C 263.0	11 37 09.3	66 04 28	0.652	16.32	-27.1	46.21	0.601
92	4C 56.27	18 23 14.8	56 49 18	0.664	18.5	-24.9	45.40	0.802
93	3C 380.0	18 28 13.5	48 42 40	0.691	15.81	-26.7	46.16	0.797
94	B2 0923+39	9 23 55.3	39 15 24	0.698	17.86	-25.7	45.67	0.875
95	S4 1716+68	17 16 27.9	68 39 48	0.777	18.5	-25.3	45.56	0.715
96	3C 454.3	22 51 29.5	15 52 54	0.859	16.10	-27.8	46.61	0.765
97	PG 1718+481	17 18 17.7	48 07 11	1.084	14.71	-29.9	47.36	0.312
98	NRAO 140	3 33 22.3	32 08 36	1.263	17.5	-27.6	46.67	0.752
99	3C 298.0	14 16 38.8	6 42 21	1.439	16.79	-28.7	46.88	0.654
100	PKS 2223+21	22 23 14.8	21 02 50	1.959	18.0	-28.4	46.80	0.728
101	S5 0836+71	8 36 21.6	71 04 22	2.160	16.5	-30.1	47.45	0.672
102	PKS 2149-306	21 49 00.5	-30 42 00	2.345	18.0	-28.6	46.84	0.717

⁽a) $\lambda = 5500 \text{ Å}$

objects of the ROSAT quasar sample with $\alpha_{RO} \leq 0.25$ as radio-quiet and, therefore, all sample members with $\alpha_{RO} > 0.25$ as radio-loud. In calculating the α_{RO} values given in Table 1, the visual magnitudes and the 5 GHz radio fluxes of the sources are taken from the Véron-Cetty & Véron AGN catalogue (1991). In Table 1 the objects are organized according to their radio-loudness class: the objects No.1 to No.55 are radio-quiet, the objects No.56 to No.102 are radio-loud. Within each subgroup the quasars are ordered by increasing redshift.

The optical luminosity was calculated from the K-corrected absolute visual magnitude listed by Véron-Cetty & Véron (1991) using the calibration of Matthews and Sandage (1963):

log
$$\nu L_{\nu} = -0.4 \text{ M}_{\text{V}} + 35.357 + 0.4 \text{ F}_{\nu} \text{ E(B - V)}$$

for $\nu = 5.45 \cdot 10^{14} \text{ Hz}$ or $\lambda = 5500 \text{ Å}$

The third term corrects the luminosity for Galactic absorption in the observer's frame by applying a reddening derived from the Galactic equivalent Hydrogen column density N_{H} according to $E(B-V)=0.17\ 10^{-21}\ N_{H}$ (Predehl & Schmitt, 1994). For this and throughout the paper $H_{o}=50\ km/s\cdot Mpc$ and $q_{o}=0$ is used. The Galactic column densities are taken from Stark et al. (1992). They are based on 21cm radio measurements and represent mean values averaged over sky fields ~ 3 sq.deg in size. For some quasars more accurate values obtained with narrow beam radio measurements are available (Elvis et al., 1989) which are then adopted in Table 3.

X-ray measurements with the *Einstein Observatory* in the energy band from 0.2 keV to 3.5 keV were found for 28 quasars of our sample (Wilkes & Elvis, 1987; Shastri et al., 1991; Elvis et al., 1994). Medium energy photon indices could be compiled for 14 quasars from published EXOSAT measurements (Lawson et al., 1992), whereas indices of the spectra of further 4 quasars were obtained from *Ginga* observations (Williams et al., 1992). The corresponding medium energy ranges are (2 - 10) keV and (1.7 - 17.4) keV, respectively. The photon indices are given in Table 4.

3. Analysis of ROSAT data

3.1. Data reduction

For each source of the sample a sky field of about 2 degrees in diameter of merged survey X-ray data centered on the optical position of the source was analyzed. In the all-sky survey the counts making up the X-ray image of the sky field are detected at various locations in the detector's field of view. Therefore, a vignetting correction of the registered X-ray counts is applied by attributing to each count a factor which is given by the ratio of the effective area of the telescope at the center of the field of view and the off-axis effective area corresponding to the impact point of the photon onto the detector (Aschenbach, 1988). In order to establish a count rate spectrum of a sample X-ray source, we extracted all counts from a circular area around its X-ray centroid and corrected them for the local background. This was done by using well defined procedures already often described in literature (e.g. Brinkmann & Siebert, 1994). The

radii of the source extraction areas ranged from 2 arcmin for faint sources to 4 arcmin for strong X-ray survey sources. They were determined individually for each given target source by using radial profiles. The background surface brightness near the target sources ranged from 4 10⁻⁴ to 7 10⁻⁴ cts/s arcmin². After background subtraction the resultant data consists of a gain calibrated, binned up pulse height spectrum for each sample source which has further been corrected for deadtime mainly caused by anti-coincidence events in the PSPC (Snowden et al., 1992). Energy bins lower than 0.08 keV and beyond 2.4 keV were ignored as there the instrument's response is not well known.

3.2. Adaptive hardness ratios

A reliable estimation of the parameters of ROSAT X-ray spectra by least squares fitting of model spectra folded through the instrument response function to the measured count rate spectra requires a minimum total count number of 300 cts (Walter & Fink, 1993). The pulse height spectra of half of the quasars in our sample, however, contain less than 300 counts. In order to characterize the spectral properties of these fainter sources we define adaptive hardness ratios

$$HR1 = \frac{B-A}{A+B}$$
 and $HR2 = \frac{D-C}{D+C}$,

where A, B, C, and D are the count numbers in the following energy bands

A =
$$[#8, #b]$$
, B = $[#(b+1), #240]$,
C = $[#(b+1), #c]$, D = $[#(c+1) - #240]$.

Here, the symbol "#" denotes a channel number of the pulse height spectrum. The corresponding photon energy E in units of [keV] is then approximately obtained by dividing the channel number by 100.

From these hardness ratios we estimate the photon index and the low energy absorption assuming that the ROSAT X-ray spectra of quasars are approximately described by power laws. In order to be able to handle very steep as well as heavily absorbed spectra, the hardness ratios HR1 and HR2 are constructed as adaptive quantities with variable boundaries b and c of the defining energy bands. These boundaries are determined for individual source spectra by the condition that the relative statistical error of the count numbers A, C, and D should be approximately equal. The hardness ratios are statistically independent Gaussian distributed quantities. For the sample sources they are given in Table 2 together with the sources' count rate and their survey exposure.

To determine for an assumed power law spectrum the photon index Γ_o and the equivalent Hydrogen column density N_{Ho} from the measured hardness ratios, we minimize the sum of the quadratic deviations between these hardness ratios and those calculated, with (b,c) fixed, from the model spectrum, folded through the instrument's response, as a function of Γ and N_H .

To determine the errors of the estimated spectral parameters (Γ_o , N_{Ho}) we look in the HR1/HR2-plane for the error ellipse, centered at the observed coordinates (HR1_{meas}, HR2_{meas}),

Table 2. Spectral characteristics

No.	Object	Exposure	Count rate	HR1	HR2	b	c
		[s]	[cts/s]				
1	MIZNI 500	(11	a) Radio-Qui	-	0.00 0.00	477	00
1 2	MKN 509 ESO 141-G55	644 186	4.86 ± 0.11	0.33 ± 0.02	-0.02 ± 0.03	47 60	99
3	4U 0241+61	186 915	3.03 ± 0.17 0.49 ± 0.03	0.33 ± 0.05	-0.01 ± 0.07	69	107
4	F 9	550		0.32 ± 0.06	-0.08 ± 0.08	120	156
5	MKN 926	461	3.66 ± 0.10 2.09 ± 0.09	0.32 ± 0.03 0.33 ± 0.04	-0.04 ± 0.04 -0.01 ± 0.05	33 63	91 109
6	0959-079	616	0.24 ± 0.03	0.33 ± 0.04 0.28 ± 0.12	-0.01 ± 0.03 -0.05 ± 0.14	71	111
7	F 1116	162	0.24 ± 0.03 2.11 ± 0.14	0.28 ± 0.12 0.27 ± 0.07	-0.05 ± 0.14 -0.05 ± 0.09	27	52
8	I Zw 1	626	0.95 ± 0.05	0.27 ± 0.07 0.33 ± 0.05	-0.03 ± 0.09 -0.01 ± 0.07	57	93
9	II Zw 136	619	1.48 ± 0.06	0.33 ± 0.03 0.32 ± 0.04	-0.01 ± 0.07 -0.02 ± 0.05	32	85
10	PG 0844+349	621	0.64 ± 0.05	0.32 ± 0.04 0.32 ± 0.07	-0.02 ± 0.03 -0.03 ± 0.09	34	83
11	MKN 584	584	0.64 ± 0.03 0.43 ± 0.04	0.32 ± 0.07 0.29 ± 0.09	-0.10 ± 0.03	33	93
12	MKN 478	716	5.91 ± 0.04	0.29 ± 0.09 0.29 ± 0.02	-0.08 ± 0.02	21	32
13	VII Zw 118	548	0.96 ± 0.06	0.33 ± 0.06	-0.04 ± 0.02	39	87
14	MKN 1383	497	1.38 ± 0.07	0.28 ± 0.05	-0.05 ± 0.07	30	82
15	PG 1404+226	680	0.54 ± 0.04	0.32 ± 0.07	-0.06 ± 0.09	23	36
16	PG 0804+761	554	1.65 ± 0.07	0.33 ± 0.04	-0.01 ± 0.05	36	89
17	IR 1334+2438	521	2.74 ± 0.09	0.25 ± 0.03	-0.13 ± 0.04	22	35
18	MKN 877	818	0.23 ± 0.03	0.31 ± 0.12	-0.03 ± 0.14	57	113
19	TON S210	547	0.35 ± 0.04	0.32 ± 0.10	-0.06 ± 0.13	22	42
20	PG 0906+48	702	0.44 ± 0.04	0.27 ± 0.08	-0.07 ± 0.10	24	43
21	MKN 106	492	0.26 ± 0.04	0.25 ± 0.13	-0.14 ± 0.16	27	63
22	PG 1416-129	466	0.35 ± 0.04	0.33 ± 0.11	-0.02 ± 0.13	81	116
23	MKN 876	2119	0.99 ± 0.03	0.32 ± 0.03	-0.02 ± 0.04	30	76
24	MKN 813	738	0.89 ± 0.05	0.28 ± 0.05	-0.07 ± 0.07	27	81
25	VII Zw 244	524	0.32 ± 0.03	0.32 ± 0.10	-0.02 ± 0.13	25	44
26	TON 256	951	0.49 ± 0.03	0.33 ± 0.06	-0.04 ± 0.08	46	95
27	PG 1626+554	1230	0.70 ± 0.04	0.29 ± 0.05	-0.04 ± 0.06	25	55
28	KAZ 102	25396	0.37 ± 0.01	0.33 ± 0.02	-0.01 ± 0.02	48	98
29	PG 1115+407	523	0.58 ± 0.05	0.28 ± 0.08	-0.09 ± 0.10	22	38
30	PG 0052+251	470	0.56 ± 0.05	0.32 ± 0.08	-0.01 ± 0.11	63	110
31	PG 1307+085	504	0.73 ± 0.05	0.29 ± 0.07	-0.04 ± 0.09	27	67
32	Q 0056-363	547	0.91 ± 0.06	0.32 ± 0.06	-0.01 ± 0.08	25	54
33	PG 1402+261	659	0.76 ± 0.05	0.33 ± 0.06	-0.05 ± 0.07	22	36
34	GQ COM	703	0.65 ± 0.04	0.33 ± 0.06	-0.01 ± 0.08	27	77
35	PG 1048+342	620	0.23 ± 0.03	0.23 ± 0.13	-0.15 ± 0.16	26	50
36	PG 1322+659	885	0.75 ± 0.04	0.33 ± 0.05	-0.03 ± 0.06	24	42
37	PHL 909	624	0.33 ± 0.04	0.32 ± 0.10	-0.04 ± 0.13	39	107
38	V 396HER	985	0.16 ± 0.02	0.27 ± 0.14	-0.07 ± 0.15	64	109
39	PG 1116+215	498	1.21 ± 0.07	0.25 ± 0.05	-0.11 ± 0.07	25	44
40	B 340	766	0.33 ± 0.03	0.32 ± 0.09	-0.01 ± 0.11	22	33
41	PG 0947+396	706	0.42 ± 0.04	0.33 ± 0.08	-0.06 ± 0.10	27	78
42	PG 0953+415	715	1.05 ± 0.05	0.31 ± 0.05	-0.04 ± 0.06	23	38
43	US 1329	619	0.28 ± 0.03	0.28 ± 0.10	-0.04 ± 0.13	28	79
44	US 1107	742	0.15 ± 0.03	0.29 ± 0.15	-0.06 ± 0.20	20	50
45	PG 1444-407	1041	0.43 ± 0.03	0.26 ± 0.07	-0.08 ± 0.09	24	35
46	AB 125	759	0.20 ± 0.03	0.22 ± 0.13	-0.12 ± 0.17	21	34
47	Q 0530-373	784 742	0.29 ± 0.03	0.30 ± 0.10	-0.03 ± 0.12	30	101
48	TON 83	742	0.60 ± 0.04	0.33 ± 0.06	-0.01 ± 0.08	23	35
49 50	B 337	770	0.26 ± 0.03	0.27 ± 0.11	-0.10 ± 0.13	25	98
50	CBS 56	710	0.25 ± 0.03	0.32 ± 0.11	-0.01 ± 0.14	26	56
51 52	PC 1014+4717	773	0.20 ± 0.03	0.33 ± 0.13	-0.06 ± 0.16	22 25	32 57
52 52	Q 1214+0826	640	0.25 ± 0.03	0.30 ± 0.11	-0.04 ± 0.14	25	57 20
53 54	Q 1230+0947	634	0.24 ± 0.03	0.30 ± 0.13	-0.06 ± 0.17	23	38 55
54 55	US 737 PG 1407+265	720 723	0.16 ± 0.03 0.19 ± 0.03	0.27 ± 0.16 0.18 ± 0.14	-0.05 ± 0.19 -0.15 ± 0.18	25 23	55 43
	1 0 140/1403	123	0.17 ± 0.03	U.10 ± U.14	-0.13 ± 0.10	43	713

No.	Object	Exposure	Count rate	HR1	HR2	b	С
		[s]	[cts/s] b) Radio-Loue	1 Ouggara			
	DC 1011 - 142	(20	*	0.29 ± 0.04	-0.06 ± 0.05	26	57
56	PG 1211+143	638	1.95 ± 0.07	0.29 ± 0.04 0.33 ± 0.07	-0.05 ± 0.09	85	130
57	III Zw 2	644	0.53 ± 0.04	0.33 ± 0.07 0.32 ± 0.04	-0.03 ± 0.09 -0.02 ± 0.06	96	134
58	4C 74.26	1510	0.64 ± 0.03	0.32 ± 0.04 0.32 ± 0.01	-0.02 ± 0.00 -0.03 ± 0.02	35	85
59	PKS 0558-540	1585	6.01 ± 0.08	0.32 ± 0.01 0.33 ± 0.02	-0.03 ± 0.02 -0.02 ± 0.02	27	76
60	3C 273	539	8.47 ± 0.16	0.33 ± 0.02 0.32 ± 0.07	-0.02 ± 0.02 -0.01 ± 0.09	41	93
61	PKS 2349-01	525	0.64 ± 0.05		-0.01 ± 0.09 -0.01 ± 0.09	26	79
62	B2 1028+31	668	0.51 ± 0.04	0.33 ± 0.07		82	116
63	PKS 1020-103	611	0.25 ± 0.03	0.30 ± 0.12	-0.05 ± 0.15	69	113
64	PKS 0837-12	487	0.45 ± 0.04	0.28 ± 0.09	-0.04 ± 0.12	36	91
65	B2 1721+34	1174	1.12 ± 0.04	0.32 ± 0.04	-0.03 ± 0.04	29	83
66	PKS 1217+02	546	0.40 ± 0.04	0.32 ± 0.10	-0.03 ± 0.12	23	67
67	B2 1223+25	690	0.21 ± 0.03	0.30 ± 0.13	-0.11 ± 0.16		92
68	PKS 1302-102	434	0.36 ± 0.04	0.32 ± 0.11	-0.05 ± 0.15	34	92 82
69	B2 1128+31	452	0.57 ± 0.05	0.30 ± 0.09	-0.03 ± 0.11	28	
70	B2 2201+31A	823	0.27 ± 0.03	0.33 ± 0.09	-0.02 ± 0.11	83	115
71	4C 73.18	2253	0.32 ± 0.02	0.32 ± 0.05	-0.03 ± 0.07	80	118
72	B2 1351+26	632	0.25 ± 0.03	0.32 ± 0.12	-0.01 ± 0.15	24	47
73	3C 249.1	683	0.42 ± 0.04	0.33 ± 0.08	-0.01 ± 0.10	34	96
74	PKS 1451-375	484	0.27 ± 0.04	0.32 ± 0.14	-0.03 ± 0.16	71	98
75	4C 69.18	1583	0.28 ± 0.02	0.31 ± 0.07	-0.02 ± 0.08	29	79
76	PKS 2227-399	452	0.64 ± 0.05	0.29 ± 0.08	-0.06 ± 0.10	28	88
77	LB 2136	562	0.34 ± 0.04	0.32 ± 0.10	-0.02 ± 0.12	37	86
78	PKS 1049-09	592	0.33 ± 0.04	0.28 ± 0.11	-0.05 ± 0.13	34	90
79	3C 48.0	526	0.70 ± 0.05	0.33 ± 0.07	-0.04 ± 0.09	37	101
80	B2 1512+37	936	0.32 ± 0.03	0.32 ± 0.08	-0.01 ± 0.10	24	58
81	PKS 1200-051	509	0.36 ± 0.04	0.33 ± 0.11	-0.00 ± 0.13	34	92
82	B2 1208+32A	724	0.19 ± 0.03	0.28 ± 0.13	-0.07 ± 0.17	24	53
83	4C 61.20	882	0.37 ± 0.03	0.27 ± 0.08	-0.05 ± 0.10	25	48
84	4C 09.72	657	0.22 ± 0.03	0.31 ± 0.12	-0.03 ± 0.14	68	103
85	PKS 1222+21	675	0.22 ± 0.03	0.31 ± 0.13	-0.05 ± 0.14	34	83
86	PKS 0454-22	599	0.21 ± 0.03	0.33 ± 0.13	-0.02 ± 0.16	59	106
87	3C 279	434	2.42 ± 0.10	0.33 ± 0.04	-0.01 ± 0.05	59	106
88	PKS 0405-12	531	0.53 ± 0.05	0.32 ± 0.09	-0.01 ± 0.11	49	104
89	4C 41.21	720	0.31 ± 0.03	0.31 ± 0.10	-0.04 ± 0.12	28	74
90	MC 1104+167	387	0.48 ± 0.05	0.33 ± 0.10	-0.02 ± 0.13	24	58
91	3C 263.0	948	0.41 ± 0.03	0.21 ± 0.07	-0.12 ± 0.09	26	51
92	4C 56.27	3283	0.10 ± 0.01	0.32 ± 0.10	-0.07 ± 0.10	88	128
93	3C 380.0	1845	0.19 ± 0.02	0.32 ± 0.08	-0.01 ± 0.10	85	125
94	B2 0923+39	686	0.30 ± 0.03	0.33 ± 0.10	-0.03 ± 0.12	26	85
95	S4 1716+68	5913	0.13 ± 0.01	0.32 ± 0.06	-0.02 ± 0.07	75	114
96	3C 454.3	670	0.75 ± 0.05	0.33 ± 0.06	-0.01 ± 0.07	88	132
97	PG 1718+481	1226	0.15 ± 0.02	0.28 ± 0.12	-0.05 ± 0.15	30	95
98	NARO 140	630	0.13 ± 0.02 0.22 ± 0.03	0.31 ± 0.12	-0.06 ± 0.14	110	138
99	3C 298.0	664	0.22 ± 0.03 0.37 ± 0.04	0.33 ± 0.10	-0.01 ± 0.11	58	108
	PKS 2223+21	732	0.37 ± 0.04 0.14 ± 0.02	0.33 ± 0.16	-0.05 ± 0.18	97	135
100	S5 0836+71	640	0.14 ± 0.02 0.67 ± 0.05	0.32 ± 0.07	-0.02 ± 0.08	80	118
101	PKS 2149-306	499	0.57 ± 0.05 0.54 ± 0.05	0.32 ± 0.09	-0.03 ± 0.11	51	99
102	FN3 2149-300	433	0.57 ± 0.05	0.02 1 0.07			

40

which comprises 68.3% of all Gaussian distributed coordinate pairs (HR1,HR2). This ellipse is defined by the 2-dimensional probability distribution of the hardness ratios, the projected 1σ widths are given by the statistical errors of the measured quantities:

$$\Delta HR(i) = \frac{2}{(U+V)^2} \sqrt{U^2 \Delta V^2 + V^2 \Delta U^2}$$

with
$$(U, V) = \begin{cases} (A, B) & \text{for } i = 1\\ (C, D) & \text{for } i = 2 \end{cases}$$

Among the points on the circumference of the error ellipse we search for those pairs (HR1,HR2), for which the corresponding values of (Γ, N_H) are extrema. As errors of the parameters we then define

$$\pm \Delta \Gamma = \begin{cases} \Gamma_{max} - \Gamma_o \\ \Gamma_o - \Gamma_{min} \end{cases}$$

and analogously for the N_H-value. In the case of constant, predefined N_H, the location of allowed (HR1,HR2) pairs as a function of Γ shrinks to a line in the HR1/HR2-plane. Then the errors of Γ_{o} are given by the maximum and minimum values of Γ which correspond to locations on the line, for which the minimum of the squared deviations is increased by unity.

To demonstrate that the adaptive hardness ratio technique and the least squares fit methods yield the same estimates of the spectral parameters, we checked both methods in the case of those 51 sources of our sample, whose spectra contained more than 300 cts. The least squares fits of a simple power law modified by low energy absorption to the count rate spectra were all well acceptable. We did found systematic variations of the residua near 0.8 keV and below 0.5 keV, but none of them was larger than 5 percent of the spectral value at these photon energies. There was no signature in the residua of any of the quasar spectra distinct enough to be interpreted as an spectral edge such like the oxygen K-edge identified in the spectra of several Seyfert galaxies (Nandra et al., 1993). The mean of the differences of the slopes determined with the adaptive hardness ratio method and with least squares fits is less than 15% in units of the corresponding standard deviations derived for two interesting parameters.

Both methods are stable for photon indices between 1 and 5 and for column densities up to 5 10²¹ cm⁻². For larger column densities both techniques yield consistent, but wrong results, which underestimate the N_H -value and the Γ . This effect is caused by the limited width of the ROSAT energy band as for very high absorption the inflexion point to the power law part of the spectrum is shifted outside of the ROSAT window.

Finally, it should be noted that we use a maximum likelihood algorithm described by Maccacaro et al. (1988) whenever a mean value of a measured quantity has to be calculated. This algorithm allows to deconvolve the intrinsic distribution of a quantity from the distribution of the measured observables and their errors. It is, therefore, possible to determine the mean $<\alpha>$ and the width σ_{α} of the distribution of the quantity α considered and to define their uncertainties $\Delta < \alpha >$ and $\Delta \sigma_{\alpha}$ at given levels of confidence.

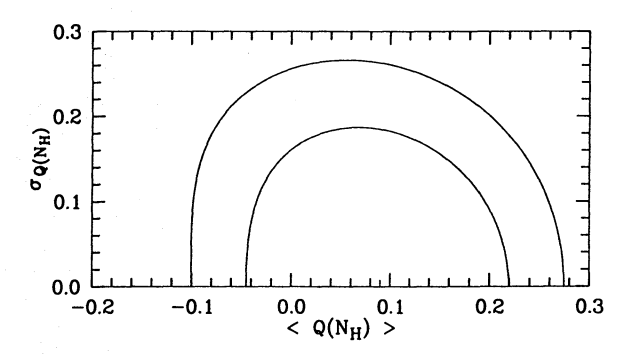


Fig. 2. Mean and width of the distribution of normalized deviations of best-fit column densities and Galactic column densities and significance contours of the 68.3% and 90% confidence levels

4. Results

For each source in our sample the adaptive hardness ratios were calculated from their X-ray spectra. Using the method described above the photon indices and the equivalent Hydrogen column densities were derived assuming that the soft X-ray spectra of the sources can well be described by absorbed power law spectra. The results are given in Table 3.

4.1. Absorbing column density

Analyzing the X-ray spectra of quasars as measured with the IPC detector onboard the Einstein Observatory in the photon energy band (0.3 - 3.5)keV, Wilkes & Elvis (1987) found that the best-fit column densities are systematically smaller than the values derived from 21 cm radio measurements. The latter we shall call the Galactic column densities N_{Hgal}. From this finding the authors concluded that a great fraction of the quasars shows an excess emission below ~ 0.3 keV. For a comparison of the best-fit column densities and the Galactic column densities of the sources of our sample we show in Fig.2 the contour diagram of the mean and the width of the normalized difference of both column densities defined as

$$Q(N_{H}) = \frac{N_{Hgal} - N_{Hfit}}{N_{Hgal}}$$

For the error of Q(N_H), which is needed for the calculation of the mean and width of Q(N_H), the uncertainties of the Galactic column densities resulting from radio measurements have to be taken into account. For the N_H values given by Stark et al. (1992) no errors are quoted. In order to obtain an average error for those values, we considered the distribution of differences between them and those reported by Elvis et al. (1989) for sources of our sample, for which both values are available. The errors of the N_H -values from Elvis et al. are claimed to be $\sim 1~10^{-19}~cm^{-2}$ or 5% whatever error is larger. The 1σ width of the difference distribution is 12%. This relative average error is attributed to each N_H-value taken from Stark et al. (1994). These resulted to < Q(N_H) >= $0.09^{+0.08}_{-0.09}$ and $\sigma_{\rm Q(N_H)} = 0.00^{+0.08}_{-0.00}$. Therefore, contrary to the sample studied by Wilkes & Elvis (1987), the best-fit N_H-values for the sources of our sample are not systematically

Table 3. Best fit parameters

No.	Object	$N_H^{(b)}$	Γ	$N_{H\ gal}^{(b)}$	$\Gamma_{N_{H \ gal}}$	$F_{0.1-2.4keV}^{(c)}$	$\nu F_{ u}^{(c)}$	$\log \nu L_{ u}^{(d)}$
1	MKN 509	$3.1^{+0.7}_{-0.6}$	2.07+0.21	a) Radio-Q4.54	Quiet Quasars 2.51 ^{+0.04}	1490 025	2.050 0.049	44.06
2	ESO 141-G55	$6.1^{+4.2}_{-2.8}$	$2.07^{+0.21}_{-0.21}$ $2.33^{+0.71}_{-0.64}$	5.08	$2.31_{-0.04}$ $2.13_{-0.12}^{+0.11}$	14.89 ± 0.35	2.050 ± 0.048	44.06 44.10
3	4U 0241+61	101^{+133}_{-82}	$2.61^{+4.22}_{-2.61}$	$73.30^{(a)}$	$1.67^{+0.35}_{-0.36}$	7.82 ± 0.43 4.22 ± 0.28	2.045 ± 0.112 2.012 ± 0.135	44.10
	F 9	2.6+0.7	2.01 -2.61		1.07 _{-0.36} 2.39+0.05			
4		$2.6^{+0.7}_{-0.6}$	$2.20^{+0.25}_{-0.24}$	3.12	$2.38^{+0.05}_{-0.05}$	7.95 ± 0.23	1.369 ± 0.039	44.10
5	MKN 926	$2.6^{+1.6}_{-1.3}$ $5.3^{+14.7}_{-4.7}$	$1.64^{+0.44}_{-0.43}$	3.57	$1.89^{+0.08}_{-0.08}$	4.10 ± 0.18	1.495 ± 0.064	44.17
6	0959-079	5.3_4.7	$2.18^{+1.75}_{-1.27}$	4.74	$2.07^{+0.25}_{-0.27}$	0.59 ± 0.07	0.167 ± 0.020	43.36
7	F 1116	$7.7^{+4.9}_{-3.6}$	$4.92^{+1.76}_{-1.34}$	2.08	$2.73^{+0.11}_{-0.11}$	3.73 ± 0.25	0.337 ± 0.023	43.73
8	IZw 1	$8.0^{+2.9}_{-2.4}$	$3.27^{+0.63}_{-0.59}$	$5.07^{(a)}$	$2.56^{+0.09}_{-0.10}$	3.24 ± 0.17	0.411 ± 0.022	43.86
9	II Zw 136	$3.3^{+1.2}_{-1.0}$	$2.54_{-0.39}^{+0.41}$	$4.20^{(a)}$	$2.83^{+0.07}_{-0.07}$	5.27 ± 0.23	0.395 ± 0.017	43.88
10	PG 0844+349	$4.8^{+2.1}_{-1.9}$	$3.00^{+0.69}_{-0.65}$	$3.39^{(a)}$	$2.54^{+0.11}_{-0.11}$	1.60 ± 0.11	0.210 ± 0.015	43.61
11	MKN 584	$2.6^{+2.3}_{-1.7}$	$2.27^{+0.80}_{-0.71}$	3.19	$2.46^{+0.14}_{-0.15}$	0.99 ± 0.09	0.149 ± 0.013	43.64
12	MKN 478	$1.9^{+0.5}_{-0.4}$	$3.43^{+0.35}_{-0.30}$	1.04	$2.82^{+0.04}_{-0.04}$	6.11 ± 0.12	0.463 ± 0.009	44.16
13	VII Zw 118	$5.4^{+1.8}_{-1.6}$	$3.05^{+0.56}_{-0.53}$	4.86	$2.87^{+0.10}_{-0.10}$	4.04 ± 0.23	0.279 ± 0.016	43.94
14	MKN 1383	$3.1^{+1.4}_{-1.2}$	$2.61^{+0.51}_{-0.46}$	$2.64^{(a)}$	$2.45^{+0.08}_{-0.08}$	2.71 ± 0.14	0.413 ± 0.021	44.17
15	PG 1404+226	$3.9^{+4.2}_{-2.5}$	$3.93^{+1.71}_{-1.12}$	$2.00^{(a)}$	$3.10^{+0.16}_{-0.14}$	1.04 ± 0.08	0.043 ± 0.003	43.34
16	PG 0804+761	$3.7^{+1.2}_{-1.1}$	$2.52^{+0.39}_{-0.38}$	$3.12^{(a)}$	$2.32^{+0.07}_{-0.07}$	3.50 ± 0.15	0.676 ± 0.029	44.52
17	IR 1334+2438	$2.0^{+1.0}_{-0.7}$	$3.33^{+0.56}_{-0.43}$	1.12	$2.80^{+0.07}_{-0.07}$	2.98 ± 0.10	0.234 ± 0.008	44.14
18	MKN 877	$0.8^{+3.3}_{-0.8}$	$1.10^{+1.05}_{-0.58}$	$4.35^{(a)}$	$2.17^{+0.23}_{-0.26}$	0.56 ± 0.07	0.137 ± 0.016	43.94
19	TON S210	$1.3^{+3.3}_{-1.2}$	$2.54^{+1.54}_{-0.80}$	1.58	$2.69^{+0.19}_{-0.18}$	0.49 ± 0.05	0.048 ± 0.005	43.53
20	PG 0906+48	$3.1_{-2.0}^{+5.0}$	$3.42^{+2.05}_{-0.99}$	1.69	$2.75^{+0.14}_{-0.13}$	0.65 ± 0.05	0.056 ± 0.005	43.61
21	MKN 106	$5.2^{+6.7}_{-3.8}$	$3.90^{+2.32}_{-1.52}$	2.09	$2.72^{+0.22}_{-0.21}$	0.46 ± 0.06	0.043 ± 0.006	43.53
22	PG 1416-129	12.5^{+67}_{-11}	2 18+4.15	$7.20^{(a)}$	$1.95^{+0.30}_{-0.33}$	0.94 ± 0.10	0.315 ± 0.035	44.41
23	MKN 876	1 2+0.9	$3.06^{+0.31}_{-0.29}$	$2.66^{(a)}$	2 40+0.05	1.98 ± 0.06	0.290 ± 0.009	44.40
24	MKN 813	$1.6^{+1.2}_{-0.9}$	2 15+0.47	2.54	$2.53^{+0.09}_{-0.09}$	1.75 ± 0.00 1.75 ± 0.10	0.235 ± 0.003 0.235 ± 0.013	44.32
25	VII Zw 244	$6.1^{+13}_{-4.4}$	$4.46^{+4.89}_{-1.87}$	1.98	$2.76^{+0.18}_{-0.17}$	0.54 ± 0.06	0.046 ± 0.005	43.63
26	TON 256	$4.4^{+2.0}_{-1.8}$	$2.52^{+0.61}_{-0.58}$	$3.77^{(a)}$	$2.76_{-0.17}^{+0.10}$ $2.34_{-0.11}^{+0.10}$	1.20 ± 0.08	0.222 ± 0.014	44.29
27		$3.0^{+1.9}_{-1.3}$	$3.10^{+0.74}_{-0.55}$	1.99	$2.67^{+0.08}_{-0.08}$			44.04
	PG 1626+554	$3.0_{-1.3}$ $3.3_{-0.4}^{+0.4}$	$2.13^{+0.13}_{-0.13}$	$5.00^{(a)}$	2.67 _0.08	1.17 ± 0.06	0.119 ± 0.006	44.04
28	KAZ 102				$2.63^{+0.03}_{-0.03}$ $3.04^{+0.16}_{-0.15}$	1.31 ± 0.02	0.146 ± 0.002	
29	PG 1115+407	$1.5^{+2.4}_{-1.1}$	$2.79^{+1.21}_{-0.71}$	1.93	3.04_0.15	1.05 ± 0.08	0.050 ± 0.004	43.84
30	PG 0052+251	$2.3^{+3.4}_{-2.2}$	$1.53^{+0.88}_{-0.82}$	$4.50^{(a)}$	$2.12^{+0.16}_{-0.17}$	1.35 ± 0.11	0.357 ± 0.030	44.63
31	PG 1307+085	$3.5^{+2.5}_{-1.8}$	$3.06^{+0.90}_{-0.72}$	$2.20^{(a)}$	$2.56^{+0.11}_{-0.11}$	1.30 ± 0.09	0.163 ± 0.012	44.33
32	Q 0056-363	$3.4^{+2.8}_{-1.7}$	$3.21^{+1.05}_{-0.73}$	1.94	$2.60^{+0.10}_{-0.10}$	1.46 ± 0.09	0.169 ± 0.010	44.39
33	PG 1402+261	$2.3^{+2.6}_{-1.3}$	$3.20^{+1.24}_{-0.72}$	$1.42^{(a)}$	$2.74^{+0.11}_{-0.11}$	0.98 ± 0.06	0.087 ± 0.005	44.12
34	GQ COM	$2.1^{+1.6}_{-1.1}$	$2.29^{+0.60}_{-0.51}$	$1.72^{(a)}$	$2.15^{+0.10}_{-0.10}$	0.89 ± 0.06	0.224 ± 0.014	44.50
35	PG 1048+342	$6.2^{+11}_{-4.6}$	$4.62^{+4.33}_{-1.95}$	2.00	$2.91^{+0.22}_{-0.21}$	0.41 ± 0.05	0.026 ± 0.003	43.63
36	PG 1322+659	$4.3^{+3.9}_{-2.0}$	$3.83^{+1.58}_{-0.89}$	2.01	$2.83^{+0.09}_{-0.09}$	1.31 ± 0.07	0.099 ± 0.005	44.20
37	PHL 909	$0.7^{+2.3}_{-0.7}$	$1.22^{+0.90}_{-0.52}$	$4.20^{(a)}$	$2.49^{+0.18}_{-0.19}$	0.95 ± 0.10	0.137 ± 0.014	44.34
38	V 396HER	$3.6^{+6.6}_{-3.5}$	$2.01^{+1.38}_{-1.19}$	4.71	$2.27^{+0.26}_{-0.28}$	0.42 ± 0.06	0.088 ± 0.012	44.16
39	PG 1116+215	$5.2^{+4.5}_{-2.4}$	$4.32^{+1.80}_{-1.04}$	$1.44^{(a)}$	$2.66^{+0.09}_{-0.09}$	1.56 ± 0.09	0.162 ± 0.009	44.46
40	B 340	$3.3^{+12}_{-2.4}$	$3.87^{+5.73}_{-1.42}$	1.07	$2.63^{+0.19}_{-0.19}$	0.34 ± 0.03	0.037 ± 0.004	43.86
41	PG 0947+396	$2.4^{+2.2}_{-1.5}$	$2.44^{+0.80}_{-0.65}$	1.58	$2.14^{+0.12}_{-0.12}$	0.55 ± 0.05	0.142 ± 0.012	44.51
42	PG 0953+415	$2.9_{-1.3}^{+2.5}$	$3.41_{-0.68}^{+1.10}$	1.14	$2.51_{-0.08}^{+0.08}$	1.14 ± 0.05	0.158 ± 0.008	44.73
43	US 1329	$2.3^{+2.9}_{-1.8}$	$2.40^{+1.05}_{-0.83}$	2.89	$2.64^{+0.18}_{-0.18}$	0.63 ± 0.07	0.069 ± 0.007	44.43
44	US 1107	$0.0^{+1.7}_{0.0}$	$1.72^{+1.01}_{-0.33}$	1.06	$2.35^{+0.28}_{-0.26}$	0.15 ± 0.02	0.027 ± 0.004	44.04
45	PG 1444-407	$8.5^{+23}_{-5.2}$	$6.33^{+11.2}_{-2.48}$	1.31	$2.79^{+0.14}_{-0.13}$	0.13 ± 0.02 0.52 ± 0.04	0.027 ± 0.004 0.042 ± 0.003	44.30
46	AB 125	$0.8^{+3.9}_{-0.8}$	$2.69^{+2.36}_{-0.90}$	0.98	$2.79_{-0.13}$ $2.81_{-0.27}^{+0.32}$	0.32 ± 0.04 0.19 ± 0.03	0.042 ± 0.003 0.015 ± 0.002	43.90
47	Q 0530-373	$0.8_{-0.8} \ 0.2_{-0.2}^{+1.6}$	$1.15^{+0.73}_{-0.30}$	2.72	$2.81_{-0.27}$ $2.20_{-0.19}^{+0.18}$	0.19 ± 0.03 0.54 ± 0.06	0.013 ± 0.002 0.127 ± 0.013	43.90
	-	0.2 _{-0.2}	1.13_0.30		2.20_0.19			44.62
48 49	TON 83 B 337	$4.7^{+8.5}_{-2.7}$	$4.34^{+3.80}_{-1.35}$ $1.26^{+0.47}_{-0.23}$	1.44	$2.72^{+0.13}_{-0.12}$	0.78 ± 0.05 0.29 ± 0.03	0.073 ± 0.005 0.120 ± 0.013	44.62 44.76
		$0.0^{+0.8}_{0.0}$	2 70+2.32	1.01	$1.79^{+0.17}_{-0.18}$			
50 51	CBS 56	$4.8^{+6.7}_{-3.5}$	$3.70^{+2.32}_{-1.42}$	1.61	$2.41^{+0.18}_{-0.17}$	0.34 ± 0.04	0.055 ± 0.006	44.52
51 52	PC 1014+4717 Q 1214+0826	$4.4_{-2.3}^{+33} 2.9_{-2.3}^{+5.3}$	$4.35^{+20.8}_{-1.00}$ $3.03^{+1.93}_{-1.07}$	0.96 1.55	$2.68^{+0.29}_{-0.26}$ $2.44^{+0.18}_{-0.17}$	0.19 ± 0.03 0.34 ± 0.04	$0.019 \pm 0.003 \\ 0.053 \pm 0.006$	44.19 44.63
				1.70		0.20 0.05	0.005 0.000	AA 50
53	Q 1230+0947	$3.1^{+19}_{-2.7}$	$3.53^{+8.14}_{-1.53}$	1.78	$2.89^{+0.26}_{-0.24}$	0.38 ± 0.05	0.025 ± 0.003	44.58
54	US 737	$2.9^{+9.0}_{-2.7}$	$3.08^{+3.24}_{-1.39}$	1.45	$2.47^{+0.25}_{-0.24}$	0.20 ± 0.03	0.030 ± 0.005	44.68
			$2.69^{+2.27}_{-0.96}$	$1.38^{(a)}$	$2.79^{+0.26}_{-0.24}$			

Table 3. (continued)

No.	Object	$N_H^{(b)}$	Γ	$N_{H\ gal}^{(b)}$	$\Gamma_{N_{Hgal}}$	$F_{0.1-2.4keV}^{(c)}$	$ u F_{ u}^{(c)}$	$\log \nu L_{ u}^{(d)}$
) Radio-L	oud Quasars	Lither		
56	PG 1211+143	$4.5^{+1.7}_{-1.3}$	$3.65^{+0.62}_{-0.52}$	$2.83^{(a)}$	$3.01^{+0.06}_{-0.06}$	5.17 ± 0.19	0.266 ± 0.010	43.99
57	III Zw 2	$1.8^{+9.1}_{-1.8}$	$0.78^{+1.11}_{-0.66}$	$6.09^{(a)}$	$1.42^{+0.22}_{-0.23}$	1.08 ± 0.08	0.676 ± 0.051	44.39
58	4C 74.26	12.9^{+28}_{-11}	$1.32^{+1.45}_{-0.88}$	11.50	$1.24^{+0.16}_{-0.17}$	1.51 ± 0.07	1.095 ± 0.050	44.72
59	PKS 0558-540	$4.6^{+0.4}_{-0.4}$	$2.89^{+0.12}_{-0.12}$	4.82	$2.97^{+0.02}_{-0.02}$	27.25 ± 0.36	1.529 ± 0.020	45.20
60	3C 273	$2.3^{+0.4}_{-0.4}$	$2.40^{+0.17}_{-0.16}$	1.79	$2.20^{+0.03}_{-0.03}$	12.07 ± 0.23	2.814 ± 0.052	45.56
61	PKS 2349-01	$3.7^{+2.1}_{-1.8}$	$2.40^{+0.68}_{-0.65}$	3.52	$2.35^{+0.11}_{-0.12}$	1.49 ± 0.11	0.272 ± 0.020	44.64
62	B2 1028+31	$1.2^{+1.5}_{-1.0}$	$1.94^{+0.62}_{-0.51}$	$1.98^{(a)}$	$2.26^{+0.12}_{-0.12}$	0.79 ± 0.06	0.167 ± 0.013	44.45
63	PKS 1020-103	17.9^{+95}_{-16}	$3.00^{+5.78}_{-1.99}$	$4.89^{(a)}$	$1.70^{+0.29}_{-0.32}$	0.52 ± 0.07	0.240 ± 0.030	44.66
64	PKS 0837-12	$3.1^{+5.3}_{-3.0}$	$1.70^{+1.10}_{-0.97}$	$5.85^{(a)}$	$2.32^{+0.21}_{-0.23}$	1.42 ± 0.14	0.274 ± 0.026	44.78
65	B2 1721+34	$3.3^{+0.9}_{-0.9}$	$2.38^{+0.32}_{-0.31}$	$3.06^{(a)}$	$2.29^{+0.06}_{-0.06}$	2.32 ± 0.08	0.467 ± 0.017	45.04
66	PKS 1217+02	$2.4^{+2.7}_{-1.8}$	$2.31_{-0.78}^{+0.94}$	$1.97^{(a)}$	$2.16^{+0.16}_{-0.16}$	0.61 ± 0.06	0.150 ± 0.015	44.68
		-1.6	-0.76		-0.10			
67	B2 1223+25	$0.8^{+2.8}_{-0.8}$	$2.09^{+1.22}_{-0.68}$	1.73	$2.51^{+0.22}_{-0.21}$	0.31 ± 0.04	0.042 ± 0.006	44.28
68	PKS 1302-102	$2.8^{+3.2}_{-2.3}$	$2.25^{+1.08}_{-0.96}$	3.27	$2.41^{+0.19}_{-0.20}$	0.81 ± 0.10	0.134 ± 0.016	44.83
69	B2 1128+31	$1.8^{+2.2}_{-1.4}$	$2.15^{+0.82}_{-0.68}$	2.22	$2.31_{-0.14}^{+0.14}$	0.94 ± 0.08	0.184 ± 0.016	44.97
70	B2 2201+31A	29.0_{-25}^{+78}	$3.54_{-2.07}^{+4.64}$	$9.91^{(a)}$	$2.22^{+0.29}_{-0.31}$	1.01 ± 0.10	0.229 ± 0.022	45.09
71	4C 73.18	$7.0^{+11.4}_{-4.1}$	$1.97^{+0.99}_{-0.69}$	7.86	$2.07^{+0.16}_{-0.16}$	0.95 ± 0.05	0.272 ± 0.015	45.16
72	B2 1351+26	$2.8^{+8.1}_{-2.4}$	$3.10^{+3.10}_{-1.21}$	1.30	$2.40^{+0.19}_{-0.19}$	0.29 ± 0.04	0.049 ± 0.006	44.48
73	3C 249.1	$1.7^{+1.9}_{-1.4}$	$1.76^{+0.70}_{-0.65}$	$2.92^{(a)}$	$2.21_{-0.14}^{+0.14}$	0.82 ± 0.07	0.188 ± 0.016	45.04
74	PKS 1451-375	42.7_{-33}^{+126}	$6.00^{+8.37}_{-3.14}$	5.87	$2.43^{+0.29}_{-0.31}$	0.93 ± 0.13	0.148 ± 0.020	44.97
		233	3.14		-0.51			
75	4C 69.18	$3.0^{+2.0}_{-1.5}$	$2.59^{+0.69}_{-0.60}$	$2.66^{(a)}$	$2.48^{+0.11}_{-0.11}$	0.55 ± 0.04	0.081 ± 0.006	44.73
76	PKS 2227-399	$3.0^{+2.0}_{-1.5}$ $1.2^{+1.7}_{-1.1}$	$1.86^{+0.68}_{-0.57}$	1.20	$1.86^{+0.12}_{-0.12}$	0.75 ± 0.06	0.285 ± 0.023	45.22
		1.1	0.57					
77	LB 2136	$4.9^{+3.1}_{-2.6}$	$2.93^{+0.97}_{-0.89}$	1.99	$1.95^{+0.15}_{-0.16}$	0.51 ± 0.05	0.171 ± 0.018	45.04
78	PKS 1049-09	$3.0^{+2.9}_{-2.1}$	$2.38^{+0.97}_{-0.86}$	3.29	$2.49^{+0.17}_{-0.17}$	0.78 ± 0.08	0.110 ± 0.012	44.95
79	3C 48.0	$1.5^{+1.6}_{-1.2}$	$1.63^{+0.59}_{-0.55}$	$4.35^{(a)}$	$2.60^{+0.12}_{-0.12}$	2.20 ± 0.15	0.259 ± 0.018	45.40
80	B2 1512+37	$1.8^{+2.6}_{-1.3}$	$2.50^{+1.03}_{-0.68}$	1.40	$2.33^{+0.13}_{-0.13}$	0.40 ± 0.03	0.075 ± 0.006	44.84
81	PKS 1200-051	$2.4_{-2.0}^{+2.8}$	$2.04^{+0.93}_{-0.84}$	2.83	$2.20_{-0.18}^{+0.17}$	0.68 ± 0.07	0.157 ± 0.017	45.17
82	B2 1208+32A	$2.1_{-2.0}^{+6.3}$	$2.82^{+2.41}_{-1.09}$	1.45	$2.50^{+0.21}_{-0.21}$	0.24 ± 0.03	0.034 ± 0.005	44.57
83	4C 61.20	$4.0^{+5.3}_{-2.5}$	$3.65^{+2.04}_{-1.10}$	0.97	$2.27^{+0.12}_{-0.12}$	0.37 ± 0.03	0.077 ± 0.006	44.98
84	4C 09.72	$8.6^{+33}_{-6.2}$	$2.94^{+2.88}_{-1.40}$	4.07	$2.02^{+0.22}_{-0.24}$	0.48 ± 0.06	0.147 ± 0.018	45.24
85	PKS 1222+21	$5.0_{-3.1}^{+3.9}$	$3.09_{-1.07}^{+1.20}$	2.27	$2.19^{+0.20}_{-0.20}$	0.36 ± 0.05	0.087 ± 0.011	45.05
86	PKS 0454-22	$3.0^{+5.5}_{-3.0}$	$1.84^{+1.34}_{-1.17}$	3.08	$1.85^{+0.22}_{-0.25}$	0.39 ± 0.05	0.148 ± 0.020	45.44
87	3C 279	$2.8^{+1.5}_{-1.2}$	$1.77^{+0.41}_{-0.40}$	$2.22^{(a)}$	$1.60^{+0.07}_{-0.07}$	3.70 ± 0.15	1.916 ± 0.080	46.51
88	PKS 0405-12	$1.8^{+2.6}_{-1.8}$	$1.61^{+0.83}_{-0.78}$	3.87	$2.26^{+0.15}_{-0.16}$	1.25 ± 0.11	0.265 ± 0.024	45.84
		-1.0	-0.76		-0.10			
89	4C 41.21	$3.4^{+3.3}_{-2.2}$	$2.85^{+1.11}_{-0.89}$	1.21	$2.00^{+0.15}_{-0.15}$	0.36 ± 0.04	0.113 ± 0.011	45.49
90	MC 1104+167	$1.9^{+3.6}_{-1.6}$	$2.55^{+1.41}_{-0.83}$	1.53	$2.39^{+0.16}_{-0.16}$	0.63 ± 0.07	0.106 ± 0.011	45.59
91	3C 263.0	$4.9^{+4.8}_{-2.6}$	$4.09^{+1.79}_{-1.10}$	$0.82^{(a)}$	$2.28^{+0.11}_{-0.11}$	0.38 ± 0.03	0.077 ± 0.006	45.46
92	4C 56.27	$8.6^{+44}_{-7.8}$	$1.63^{+2.44}_{-1.11}$	4.14	$1.18^{+0.25}_{-0.27}$	0.19 ± 0.02	0.142 ± 0.013	45.50
93	3C 380.0	$4.4^{+23}_{-4.4}$	$1.28^{+1.65}_{-0.98}$	$6.60^{(a)}$	$1.55^{+0.25}_{-0.27}$	0.41 ± 0.03	0.227 ± 0.019	45.82
94	B2 0923+39	$0.8^{+2.0}_{-0.8}$	$1.70^{+0.82}_{-0.58}$	$1.69^{(a)}$	$2.08^{+0.17}_{-0.17}$	0.40 ± 0.04	0.114 ± 0.012	45.65
95	S4 1716+68	$5.4^{+5.6}_{-3.0}$	$1.95^{+0.74}_{-0.63}$	4.36	$1.76^{+0.17}_{-0.14}$	0.27 ± 0.02	0.115 ± 0.007	45.70
96	3C 454.3	$1.3^{+6.3}_{-1.3}$	$0.54_{-0.49}^{+0.84}$	$7.13^{(a)}$	$1.30_{-0.20}^{+0.19}$	1.57 ± 0.10	1.081 ± 0.065	46.66
		1.5	0.45		0.20			
97	PG 1718+481	$0.9^{+2.5}_{-0.9}$	$1.60^{+1.00}_{-0.65}$	2.28	$2.16^{+0.20}_{-0.21}$	0.24 ± 0.03	0.061 ± 0.008	45.91
98	NARO 140	$213.^{+142}_{-161}$	$8.82^{+3.92}_{-6.39}$	$14.22^{(a)}$	$0.72^{+0.48}_{-0.50}$	0.53 ± 0.06	0.543 ± 0.067	46.54
99	3C 298.0	$2.0^{+3.2}_{-2.0}$	$1.53^{+0.89}_{-0.83}$	$2.06^{(a)}$	$1.54^{+0.16}_{-0.17}$	0.56 ± 0.05	0.306 ± 0.030	46.73
100	PKS 2223+21	24.4^{+156}_{-25}	$1.83^{+6.99}_{-1.83}$	4.37	$0.68^{+0.47}_{-0.54}$	0.25 ± 0.04	0.267 ± 0.042	46.61
101	S5 0836+71	$6.4^{+16}_{-4.6}$	$1.86^{+1.33}_{-0.86}$	2.78	$1.25^{+0.14}_{-0.15}$	1.08 ± 0.07	0.779 ± 0.053	47.45
102	PKS 2149-306	$3.7^{+3.0}_{-2.3}$	$2.24^{+0.84}_{-0.79}$	2.05	$1.71^{+0.13}_{-0.13}$	0.80 ± 0.07	0.366 ± 0.032	47.46

 $^{^{(}a)} \text{: Elvis et al. (1989); } ^{(b)} \text{: Unit [} 10^{20} cm^{-2} \text{]; } ^{(c)} \text{: Unit [} 10^{-11} \ erg \ cm^{-2} \ s^{-1} \ at \ 2keV \text{];} ^{(d)} \text{: Unit [} erg \ s^{-1} \text{] } at \ 2keV \text{]}$

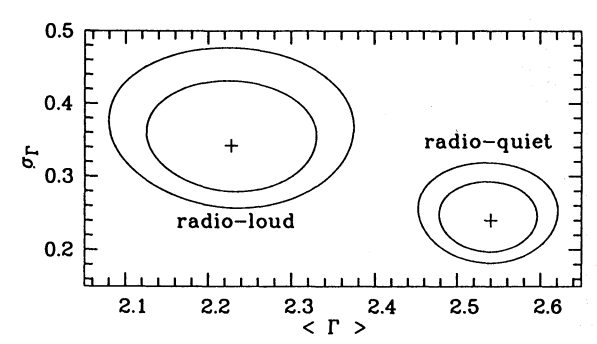


Fig. 3. Means and widths of the distributions of photon indices of the soft X-ray spectra of radio-loud and radio-quiet quasars with z < 0.6 for the low energy absorption fixed to the Galactic value. Significance contours for the confidence levels 68.3% and 90%.

smaller than the corresponding Galactic column densities, but consistent with them. This consistency motivated us to determine the photon indices of the sources' X-ray spectra with the low energy absorption fixed to the Galactic N_H value, which yields appreciably smaller errors of the single fit parameter Γ . Such a consistency between the fit N_H -value and the Galactic value has also been found in other studies of ROSAT measured AGN spectra (Walter & Fink, 1993; Laor et al., 1994; Fiore et al., 1994). The power law photon index for fixed Galactic column density is given in Table 3 for all sources together with the flux in the ROSAT energy band (0.1 - 2.4)keV corrected for low energy absorption, and the spectral flux density, and the luminosity at 2 keV. The latter is defined in the source's frame using the K-correction derived by Schmidt & Green (1986).

In the following sections we will, firstly, derive the sample mean of the power law indices for the ROSAT sample, in order to compare it with average indices found with other experiments for higher photon energies. Then we will study the soft X-ray indices of the ROSAT sources as a function of their redshifts.

4.2. Mean spectral index of the ROSAT sample

4.2.1. Spectral index and radio-loudness

It is well known from literature (Della Ceca et al., 1994, and references therein) that the medium energy X-ray spectra of radio-loud quasars are clearly flatter than those of radio-quiet QSOs. We checked our ROSAT sample for such a difference in the slope of the soft X-ray spectra of both classes of quasars. Our sample contains only rather nearby radio-quiet objects. On the other hand, a third of the radio-loud objects in the sample have redshifts greater than z = 0.6. To study comparable subgroups and to keep a possible effect of the redshift low, we therefore restrict the comparison of both quasar classes on sample members with z < 0.6. Then the radio-quiet subgroup contains 53 and the radio-loud one 33 sources. Thereby 2U 0241+61 had to be excluded because its Galactic column density exceeds the critical limit of $5 ext{ } 10^{21} ext{ } \text{cm}^{-2}$. The mean value of the photon indices and the width of their distribution is given for both radio classes in Table 5 and Fig.3. Thus we are able

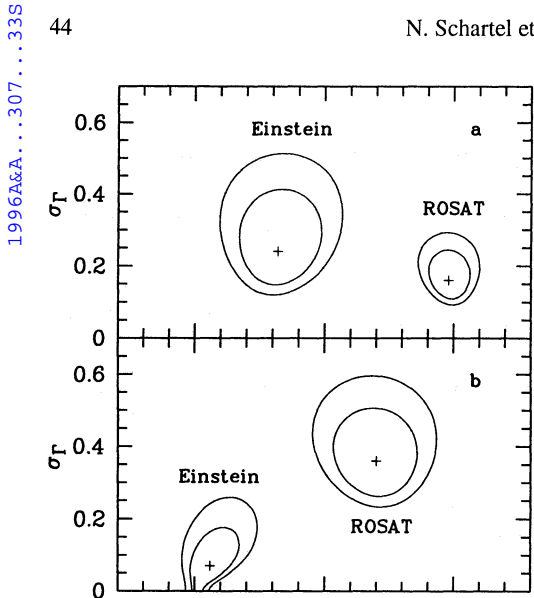
Table 4. Sources with previously measured spectral indices

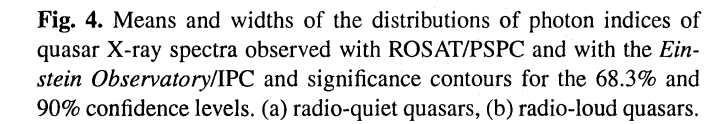
No.	Object		Pho	ton Index	
		Einstein Ob.	Ref.	EXOSAT ⁴	Ginga ⁵
		(0.3 - 3.5)keV		(2 - 10)keV	(2 - 20)keV
3	4U 0241+61			$1.7^{+0.1}_{-0.1}$	
4	F9	$1.9^{+0.2}_{-0.1}$	2	$1.9^{+0.1}_{-0.1}$	
8	I Zw 1	$2.9^{+1.7}_{-0.8}$	2	···	
9	II Zw 136	$1.81^{+0.07}_{-0.07}$	2	$2.2^{+0.2}_{-0.2}$	
10	PG 0844+349	$1.53^{+0.62}_{-0.34}$	2	<u>.</u>	
14	MKN 1383	$2.12^{+0.1}_{-0.1}$	2	$1.5^{+0.2}_{-0.2}$	
16	PG 0804+761	$2.01^{+0.51}_{-0.45}$	2		$2.00^{+0.27}_{-0.14}$
22	PG 1416-129	$1.9^{+0.5}_{-0.5}$	2		$1.08^{+0.14}_{-0.12}$
23	MKN 876	$2.10^{+0.2}_{-0.3}$	2		
28	KAZ 102	$0.8^{+0.4}_{-0.3}$	2		
30	PG 0052+251	$2.1_{-0.6}^{+1.7}$	2	$2.1_{-0.3}^{+0.3}$	
31	PG 1307+085	$1.9^{+0.5}_{-0.2}$	2		$2.26^{+0.37}_{-0.28}$
34	GQ Com	$2.1^{+0.2}_{-0.4}$	2		
37	PHL 909	$1.41^{+0.07}$	2	$1.2^{+0.3}_{-0.3}$	
39	PG 1116+215	$2.0^{+0.3}_{-0.2}$	2	*	
56	PG 1211+143	$2.8^{+0.5}_{-0.4}$	1	$2.1^{+0.1}_{-0.1}$	
57	III Zw 2	$1.4^{+0.9}_{-0.3}$	2	$1.6^{+0.1}_{-0.1}$	
59	PKS 0558-540			$2.2^{+0.2}_{-0.2}$	
60	3C 273	$1.47^{+0.03}_{-0.03}$	2	$1.6^{+0.1}_{-0.1}$	
62	B2 1028+31	$1.62^{+0.06}_{-0.06}$	2		
63	PKS 1020-103	$1.80^{+0.7}_{-1.6}$	3		
64	PKS 0837-12	$1.65^{+0.27}_{-0.23}$	2		
65	B2 1721+34	$1.5^{+0.4}_{-0.3}$	2		
66	PKS 1217+02	$1.5^{+0.5}_{-0.2}$	1	$1.8^{+0.3}_{-0.3}$	
69	B2 1128+31	$1.7^{+0.5}_{-0.4}$	3		
70	B2 2201+31A				$1.73^{+0.34}_{-0.26}$
71	4C 73.18			$2.1_{-0.3}^{+0.3}$	
73	3C 249.1	$2.0_{-0.3}^{+0.3}$	2		
79	3C 48.0	$1.7^{+0.4}_{-0.4}$	2		
87	3C 279	$1.6^{+0.2}_{-0.3}$	1		
91	3C 263.0	$1.7^{+0.4}_{-0.1}$	2	$1.8^{+0.3}_{-0.3}$	
94	B2 0923+39	$1.4^{+0.2}_{-0.2}$	1		
98	NRAO 140			$1.6^{+0.2}_{-0.2}$	

- (1) Wilkes & Elvis (1987) (2) Elvis et al.(1994)
- (3) Shastri et al. (1992) (4) Lawson et al. (1992)
- (5) Williams et al. (1992)

Table 5. Mean spectral indices of radio-loud and radio-quiet quasars

ROSAT sample	Number	$<\Gamma_{N_{\rm H}}{}_{gal}>$	$\sigma_{\Gamma_{N_{H}}}$ gal
radio-quiet	53	$2.54^{+0.04}_{-0.04}$	$0.24^{+0.03}_{-0.03}$
radio-loud	33	$2.23^{+0.07}_{-0.07}$	$0.34^{+0.08}_{-0.06}$
$\Delta\Gamma(Q-L)$	-	0.31 ± 0.08	





>

2.5

2 < Г

1.5

to confirm that in the ROSAT sample the mean spectrum of radio-quiet quasars is clearly steeper than those of the radioloud sources. The difference of their mean spectral indices is $\Delta\Gamma(Q - L) = <\Gamma_{rq}> - <\Gamma_{rl}> = 0.31 \pm 0.08.$

The mean index of $<\Gamma_{\rm rl}>=2.23\pm0.07$, which we found for the radio-loud quasars of our ROSAT sample, is consistent with the 90% confidence range of 2.10 to 2.33 of the mean index of a sample of 98 radio-loud quasars from the Kühr et al. catalogue (1979) also observed in the ROSAT all-sky survey (Brunner et al., 1992).

4.2.2. Comparison with other samples

In the following we want to compare the mean spectral indices of the ROSAT quasars, determined in the soft (0.1 - 2.4)keV energy band, with those of other samples observed at higher photon energies. Several quasar samples were observed with the Einstein Observatory using the IPC as focal plane detector. For our comparison we choose the largest Einstein quasar sample reported by Wilkes & Elvis (1987) and Elvis et al. (1994). At medium energies samples were observed with EXOSAT/ME, ((2 - 10)keV, Lawson et al., 1992), as well as with Ginga/LAC, ((2 - 20)keV, Williams et al., 1992). Using published values we determined the mean indices for the radio subgroups of these samples in the same manner as we did it for the ROSAT sample. The results are given in Table 6.

Inspecting Table 6 it can be seen that the ROSAT mean indices are greater for radio-quiet as well as radio-loud quasars than the indices of any other experiment sensitive in harder energy bands. It is further obvious that the power law indices in the Einstein band behave like those determined at medium

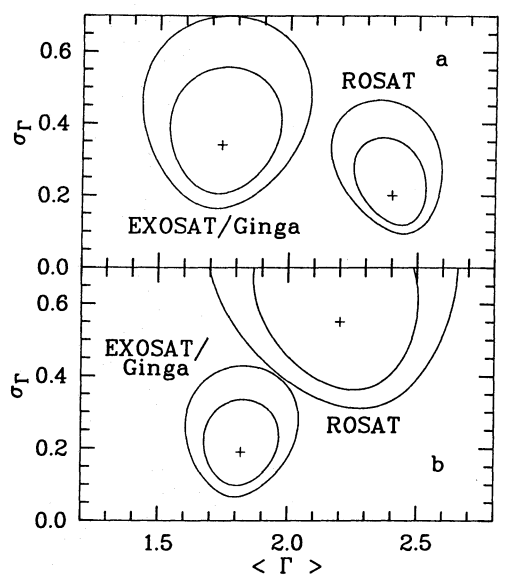


Fig. 5. Means and widths of the distributions of photon indices of quasar X-ray spectra observed with ROSAT/PSPC and with EXOSAT and Ginga, and significance contours for the 68.3% and 90% confidence levels. (a) radio-quiet quasars, (b) radio-loud quasars.

energies. In addition, the mean indices in the EXOSAT and in the Ginga bands are consistent with each other.

In order to make the comparison more specific we now restrict it to identical subgroups of all the samples, i.e. we compare the mean indices of those quasars which can be found in the ROSAT sample as well as in the other samples. The sources belonging to these subgroups can be identified in Table 4. To enhance the statistical significance of the comparison between the ROSAT subsamples and those observed at medium energies we enriched the EXOSAT subsamples with Ginga sources. The results of the comparison is given in Table 7 and in the contour diagrams of Fig.4 and Fig.5. It is again obvious that the mean indices in ROSAT soft energy band are always steeper than in any harder energy band. For the radio-quiet quasars there is a gradual flattening with increasing hardness of the energy band for which the index was determined. For the radio-loud quasars the graduality of the change in index with photon energy is not as evident as for the radio-quiet objects. Nevertheless, it can be stated also for the radio-loud subclass that there is a considerable spectral steepening towards soft X-ray wavelengths. It is remarkable that the differences between the mean indices in the ROSAT band and those at higher energies are statistically identical for radio-loud as well as for radio-quiet quasars.

Firstly, we consider that the discrepancy in the mean indices might be caused by a selection effect, if ROSAT detected preferentially quasars with steep spectra. In that case, the sources of the common subset should show on average steeper spectra than the sources in the full sample observed at higher energies. For the case of the Einstein sample, the (0.3 - 3.5)keV mean indices of the subset and the full sample are consistent with each other for radio-quiet as well as for radio-loud quasars. Therefore, we can exclude that the difference of mean indices obtained with

Table 6. Comparison of mean spectral indices of quasar samples observed with different experiments

Sample	Energy band	Total	Rad	io-Quiet	Rad	io-Loud
	[keV]	Number	Number	Index	Number	Index
ROSAT/PSPC	0.1 - 2.4	86	53	2.54 ± 0.04	33	2.23 ± 0.07
Einstein/IPC	0.3 - 3.5	33	18	$1.91^{+0.63}_{-0.36}$	15	$1.48^{+0.63}_{-0.36}$
EXOSAT/ME	2 - 10	31	13	1.91 ± 0.08	18	1.74 ± 0.07
Ginga/LAC	2 - 20	12	5	$1.93^{+0.17}_{-0.15}$	7	1.69+0.11

Table 7. Comparison of mean indices determined for identical subsamples at different energies

	Number	$<\Gamma_{ m ROSAT}>$	$<\Gamma_{Einstein}>$	$\Delta\Gamma(R-E)$
radio-quiet	15	$2.49^{+0.04}_{-0.06}$	$1.83^{+0.10}_{-0.10}$	0.66 ± 0.11
radio-loud	14	$2.20^{+0.10}_{-0.11}$	$1.56^{+0.07}_{-0.05}$	0.68 ± 0.12
	Number	$<\Gamma_{ m ROSAT}>$	$<\Gamma_{{ m EXO}/Ginga}>$	$\Delta\Gamma(R - EXO)$
radio-quiet	9	$2.40^{+0.08}_{-0.09}$	$1.74^{+0.15}_{-0.13}$	0.66 ± 0.17
radio-loud	9	$2.20^{+0.20}_{-0.21}$	$1.82^{+0.09}_{-0.09}$	0.38 ± 0.23

ROSAT and with the *Einstein Observatory* is caused by such a selection effect. For the comparison with the other medium energy samples the argumentation is analogous. An obvious possibility to explain the different mean indices at different photon energies is a curved shape of a typical quasar spectrum being steeper at soft X-rays and flatter at medium photon energies. Extrapolating the well established medium energy power law spectra into the soft X-ray regime, an excess of soft photons was found in many Seyfert 1 galaxies and quasars (Wilkes & Elvis (1987), Kruper et al. (1990), Walter & Fink (1993)). Such a soft X-ray excess is consistent with a steepening of the X-ray spectrum towards lower photon energies as is suggested by the present study.

Finally, it should be noted that the uncertainties of $\Delta\Gamma$ given in Table 6 do not contain possible miscalibrations of the different detectors as has been studied in detail for the comparison of high-count spectra measured with the PSPC(pointing mode) and the IPC by Fiore et al. (1994). In this paper we are dealing with low-count sources detected in the ROSAT all sky survey, the photon statistics of which dominate the statistical uncertainties. An addition of a \sim 10% systematic uncertainty due to errors in the cross-calibrations of the different detectors would therefore not affect the conclusions drawn.

4.3. Redshift dependence of spectral indices

If we accept this picture of a convex curved typical quasar spectrum as suggested by the comparison of the indices in different energy bands, we expect to find a decreasing power law index in ROSAT's energy band with increasing redshift. This assumption is to be tested for the full ROSAT sample of quasars listed in Table 1. The redshift range of the radio-quiet quasars in the sample is rather limited. 51 objects range in redshift from z=0

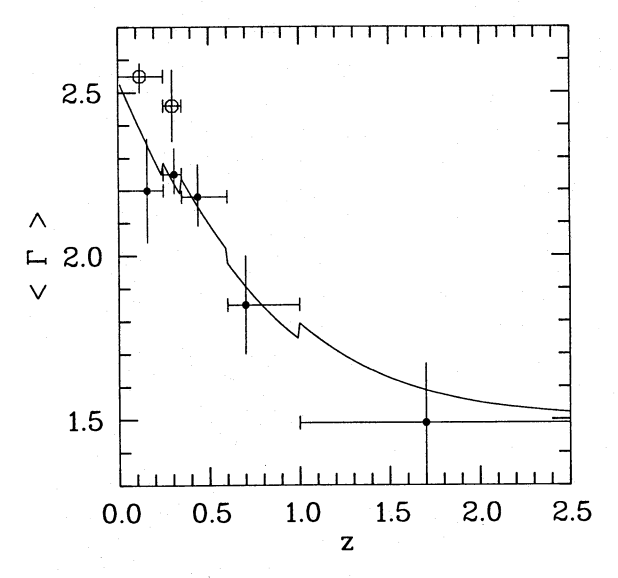


Fig. 6. Mean photon index of quasar spectra measured in the soft energy band (0.1 - 2.4)keV as a function of redshift. Filled circles: radio-loud sources; open circles: radio-quiet sources. The data points are centered on the mean redshift of the subgroup of quasars corresponding to the redshift bin. The vertical error bars represent the 1σ errors of the means $<\Gamma>$; the horizontal bars indicate the widths of the redshift bins. The solid curve decribes the redshift dependence of the spectral index for a two-component quasar spectrum.

to z=0.35 allowing to form only two redshift bins. The analysis of the redshift dependence of the power law index is, therefore, mainly performed for the subclass of radio-loud quasars, -47 objects with redshifts up to z=2.5 organized in five redshift bins. The division of the subclasses in redshift bins is indicated in Table 1. Assuming absorbed power law spectra we deter-

46

mined for all the quasars in the sample and for each redshift bin the independent spectral parameters N_H and Γ as well as photon indices $\Gamma_{\mathrm{N_H}_{gal}}$ for absorbing column densities fixed to their Galactic values. For this we used again the maximum likelihood method described in Sect. 3.2. For the calculation of $\langle N_{Hgal} \rangle$ the individual values N_{Hgal} are weighted proportional to the relative error with which the corresponding photon index could be determined. All these quantities are given for radio-quiet as well as for radio-loud sources in Table 8 and Table 9, respectively. In order to discuss optical selection effects, we additionally analyzed the X-ray spectra of radio-loud Seyfert 1 galaxies with more than 80 SASS-cts in the survey and $M_V > -23$ from the Véron-Cetty & Véron catalogue. The corresponding values are given in the redshift bin with the label 1b in Table 9. The mean indices as a function of redshift are given for both subclasses of quasars in Fig.6.

4.4. Discussion of the redshift curve

4.4.1. Selection effects

Several selection effects may affect the redshift curve in Fig.6. Here we will investigate the effects of a detection rate of soft Xray excesses varying with redshift as well as effects of a redshift dependent relative strength of the visible and of the hard X-ray spectral component. From the recent finding that stronger soft excesses are preferrably detected when the hard X-ray component is faint compared to the ultraviolet emission (Walter & Fink, 1993) it is clear that the relative strength of the hard X-ray spectrum can influence the shape of the redshift curve. In the following we will restrict our discussion to radio-loud sources, because there are data available up to higher redshifts. In a further section we will compare the results for radio-loud and radio-quiet quasars. The criteria defining our quasar sample impose strong selection effects on the ratio of optical to X-ray fluxes observable at a given redshift. At low redshifts, optical-quiet sources with a small $|\alpha_{OX}|$ are not contained in our sample as objects fainter than $M_V = -23$ were excluded (quasar definition). At high redshifts, X-ray quiet sources with large $|\alpha_{OX}|$ are under-represented as the sample is flux limited in X-rays (80 SASS-cts condition). Together, both effects will cause a decrease of the mean ratio of optical to X-ray fluxes with increasing redshift. In other words, if the strength of the soft Xray excess is related with α_{OX} , the selection effects cause that the observed soft X-ray spectra are, on average, steeper than expected at low redshifts and flatter than expecected at high redshifts.

Another selection effect, which affects the mean $|\alpha_{OX}|$ in a reshift bin, is present if the fraction of beamed sources increases with increasing redshift. Such an effect could be supposed as the detection probability for sources with a low omni-directional luminosity drops for higher redshifts. An X-ray beaming effect is only selective in the same direction as the redshift curve, if the beaming factor of the soft excess component is smaller than that of the underlying X-ray continuum. This effect can be marginally observed in our sample as all its known highly

polarized quasars (HPQs) have redshifts z > 0.5 (3C 279, 4C 56.27, 3C 454.4 with a polarisation P > 3% (Wills et al., 1992)).

Excluding the extreme PG 1718+841, which shows the strongest ratio of optical to X-ray luminosities, the intrinsic range of variation of the ratio $\nu F_{\nu\ 5500\mbox{\sc A}}/\nu F_{\nu\ 2keV}$ over the sample is of the order of 20 and the mean value of this ratio decreases by about a factor of 5 between z=0.1 and z=0.5 in the direction predicted by these selection effects. Following Walter & Fink (1993), a factor of 5 in the flux ratio corresponds to a change in the soft X-ray slope of $\Delta\Gamma\approx0.5$. Therefore, a noticeable fraction of the observed flattening with increasing redshift may be caused by these selection effects.

The possibility to detect soft X-ray excesses is reduced for increasing column densities causing low energy absorption. An aborbing column density increasing with redshift could, therefore, provide a further explanation for a flattening of the X-ray spectra at higher redshifts. It is, however, rather unlikely that intervening galaxies absorb strongly the selected sources as the redshift range of these objects is quite small (Wilkes et al., 1992b). In addition, it could be shown that not all high z quasars are intrinsically absorbed (Fink & Briel, 1993). At a 68.3% confidence level, the observed N_H value averaged over the sample is less than 5% larger than the averaged Galactic column density (Fig.2). The data show no indications of an intrinsic absorption varying with redshift.

Flux ratio selection, beaming, and absorption effects cause that the mean photon indices of the soft X-ray spectra decrease with increasing redshift. Any correction of the redshift curve with respect to these selection effects will yield steeper spectra at higher redshifts and, therefore, a higher redshift for the inflexion point of the curve.

4.4.2. The redshift effect

Alternatively, the flattening of the mean soft X-ray quasar spectrum with increasing redshift can be explained by the blue shift of the observer's spectral band in the rest frame of the source. The fact that the mean spectral slope observed in radio-loud sources at high redshift agrees with the mean spectral slope measured with the Einstein Observatory, EXOSAT, and Ginga at higher photon energies in low redshift sources supports this interpretation. By adopting ad hoc a spectral shape which describes the ultraviolet to medium X-ray spectrum in a uniform way, we can try to model the derived redshift dependence of the soft X-ray spectral slope. Previous studies of the spectra of Seyfert 1 galaxies measured simultaneously at far UV and Xray wavelengths (Walter et al., 1994) suggest a special spectral representation. This ad hoc model represents the ultravioletto-X-ray bump by a power law spectrum in the UV and EUV range modified by an exponential cut-off to meet the steep AGN soft X-ray spectrum. The medium energy spectrum is best represented by a power law, as numerous measurements of AGN spectra with Ginga demonstrated (e.g. Nandra & Pounds, 1994). Both spectral components are combined to give a representative

Table 8. Spectral parameters of radio-quiet quasars as a function of redshift

Bin	Туре	Redsh	nift	Number	< N _H >	< Γ >	$<$ N_{H}_{gal} $>$	$<\Gamma_{N_{\rm H}}{}_{gal}>$	$\langle \frac{\nu L_{opt}}{\nu L_{2keV}} \rangle$	
		Interval	< z >		$10^{20} cm^{-2}$		$10^{20} cm^{-2}$	8	280 4	
1	QSO	0.00-0.25	0.12	42	$2.89^{+0.22}_{-0.21}$	$2.56^{+0.10}_{-0.11}$	$2.87^{+0.20}_{-0.21}$	$2.55^{+0.04}_{-0.05}$	8.79	
2	QSO	0.25-0.35	0.30	9	$0.14^{+0.45}_{-0.14}$ *	$1.47^{+0.28}_{-0.27}$	$1.38^{+0.16}_{-0.16}$	$2.46^{+0.11}_{-0.11}$	6.50	

^{*} contaminated by lower limits (see Table 2)

Table 9. Spectral parameters of radio-loud quasars as a function of redshift

Bin	Туре	Redsl	nift	Number	< N _H >	< Γ >	$< N_{Hgal} >$	$<\Gamma_{ m N_{H}}{}_{ m gal}>$	$\langle \frac{\nu L_{opt}}{\nu L_{2keV}} \rangle$
		Interval	< z >		$10^{20} cm^{-2}$		$10^{20} cm^{-2}$	8	280 4
1	QSO	0.00-0.25	0.16	11	$3.23^{+0.52}_{-0.53}$	$2.52^{+0.16}_{-0.23}$	$4.12^{+0.72}_{-0.68}$	$2.20^{+0.16}_{-0.16}$	3.29
1b	QSO+AGN	0.00-0.25	0.13	18	$3.36^{+0.49}_{-0.50}$	$2.37^{+0.17}_{-0.20}$	$5.10^{+0.71}_{-0.67}$	$2.12^{+0.12}_{-0.12}$	2.49
2	QSO	0.25-0.35	0.31	12	$2.09^{+1.11}_{-1.13}$	$2.20^{+0.26}_{-0.25}$	$3.52^{+0.72}_{-0.70}$	$2.25^{+0.08}_{-0.06}$	4.06
3	QSO	0.35-0.60	0.44	10	$2.32^{+0.71}_{-0.62}$	$1.96^{+0.26}_{-0.26}$	$2.61_{-0.36}^{+0.37}$	$2.18^{+0.10}_{-0.09}$	4.32
4	QSO	0.60-1.00	0.70	8	$1.98^{+1.10}_{-1.07}$	$1.79^{+0.39}_{-0.34}$	$3.22^{+0.84}_{-0.79}$	$1.85^{+0.15}_{-0.15}$	2.89
5	QSO	1.00-2.50	1.70	6	1.95 ^{+1.35} _{-1.31}	$1.87^{+0.43}_{-0.45}$	$2.19^{+0.13}_{-0.11}$	$1.49^{+0.18}_{-0.21}$	5.57

mean ultraviolet-to-hard X-ray spectrum.

$$\frac{dN}{dE} = A_1 \left(\frac{E}{E_1}\right)^{-\Gamma_1} + A_2 \left(\frac{E}{E_2}\right)^{-\Gamma_2} exp\left(-\frac{E-E_2}{\epsilon_{cut}}\right)$$

The power law index of the medium energy component is fixed to $\Gamma_1 = 1.5$ following the measurements of quasar spectra with the Einstein/IPC in the (0.3 - 3.5)keV energy band (Wilkes & Elvis, 1987). As reference energy for this harder component we choose $E_1 = 2 \text{ keV}$. The bump component is described by a fixed power law index $\Gamma_2 = 1.4$ (Walter et al., 1994), by a corresponding reference energy which is choosen to be $E_2 = 0.009 \text{ keV}$ (1375 Å), and by a cut-off energy $\epsilon_{\rm cut}$, which is a free parameter in the modelling. The UV index of 1.4 corresponds to the flattest ultraviolet spectra oberved with IUE (Paltani & Courvoisier, 1994) and to a typical far ultraviolet spectral slope predicted by accretion disk models (Ross et al., 1992; Dörrer et al., 1992). As steeper ultraviolet spectra lead to higher cut-off energies (Walter et al., 1994), the ultraviolet spectral slope of 1.4 yields lower limits of the cut-off energy. The model spectrum is then finally defined by specifying $\epsilon_{\rm cut}$ and the ratio of normalizations at the given reference energies:

$$R = log \left(\frac{\nu F_{\nu}(0.009 \text{ keV})}{\nu F_{\nu}(2 \text{ keV})} \right)$$

For the analysis of the redshift diagram we simulated for each redshift bin and for given values of the parameters (R, ϵ_{cut}) the two-component model spectrum, redshifted it according to the mean redshift of the bin and modified it by a low energy absorption factor $\exp(-\sigma(E)\cdot < N_{Hgal}>)$, where $\sigma(E)$ is the photoelectric absorption cross section and $< N_{Hgal}>$ is the

mean Galactic column density for the redshift bin considered (Table 9). The spectra are then folded through the instrument's response function. From the resulting count rate spectra per bin adaptive hardness ratios are derived following the prescription given in Sect. 3.2. Returning to the initial assumption, on which the redshift diagram in Fig.6 was based, namely that the soft X-ray spectra of quasars can adequately be described by a simple power law, we determined from the hardness ratios the photon indices Γ_i (i = 1,5) for fixed Galactic column densities < N_{Hgal} $>_{i}$. These indices extracted for the twocomponent model spectrum are compared with the measured indices (Table 9) for all redshift bins by means of a least squares fit procedure with $(R, \epsilon_{\text{cut}})$ as free parameters. The closest approximation of the redshift diagram was achieved for a best fit ratio $log R_o = 0.23^{+0.54}_{-0.39}$ and for a best fit cut-off energy of $\epsilon_{\rm cuto} = 110^{+50}_{-34}$ eV. The goodness of the fit, presented in Fig.6 as the solid line, is characterized by $\chi^2/d.o.f. = 2.16/3$. The corresponding significance contours can be found in Fig.7. It should be noted that the discontinuities of the fit solution at the boundaries of the redshift bins (Fig.6) are caused by the different mean absorption column densities $\langle N_{Hgal} \rangle_i$ (i = 1,5). This kind of fit technique allows to determine the range of mean parameters permitted by the observed redshift curve. It can also be used to test the effects of selection and to check the predictions made by accretion disk models. A simple test of the influence of the selection effects is to assume that a fraction f_i of the sources detected in redshift bin i does not show any soft X-ray excess, i.e. their soft X-ray spectra has the medium energy spectral index of 1.5, whereas the rest of the sample sources remain unchanged. The best fit parameters are then determined by minimizing χ^2 =

Table 10. Model parameters of the redshift curve for different fractions of sample sources without ultraviolet-to-X-ray bumps

Fraction	$\epsilon_{ m cut}$	$\log\left(\frac{A_2(0.009 \text{ keV})}{A_1(2 \text{ keV})}\right)$	$\log\left(\frac{\nu F_{\nu}(0.009 \text{ keV})}{\nu F_{\nu}(2 \text{ keV})}\right)$	$\chi^2/d.o.f.$
f_i	[eV]		(,	(d.o.f.=2)
0.1	120^{+66}_{-42}	$4.82^{+0.62}_{-0.41}$	$0.13^{+0.62}_{-0.41}$	0.63
0.2	132^{+83}_{-46}	$4.72^{+0.55}_{-0.41}$	$0.026^{+0.55}_{-0.41}$	0.54
0.3	145^{+133}_{-56}	$4.64^{+0.57}_{-0.44}$	$-0.054^{+0.57}_{-0.44}$	0.50
0.4	165^{+144}_{-67}	$4.52^{+0.57}_{-0.36}$	$-0.17^{+0.57}_{-0.36}$	0.50
0.5	191^{+187}_{-43}	$4.42^{+0.23}_{-0.30}$	$-0.27^{+0.23}_{-0.30}$	0.56
0.6	251^{+236}_{-133}	$4.26^{+0.57}_{-0.21}$	$-0.43^{+0.57}_{-0.21}$	0.69
0.7	316 ⁺³²³ ₋₁₈₇	$4.18^{+0.75}_{-0.19}$	$-0.51^{+0.75}_{-0.19}$	0.93
0.8	380^{+468}_{-245}	$4.14^{+0.56}_{-0.15}$	$-0.55^{+0.56}_{-0.15}$	1.32

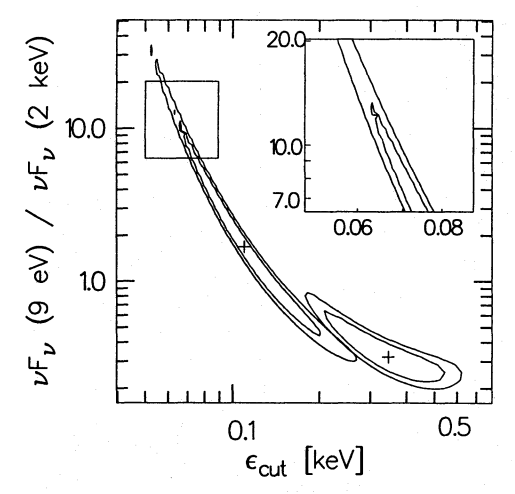


Fig. 7. Significance contours of the fit of redshifted two-component model spectra to the power law indices derived from the hardness ratios of the mean spectra determined for each redshift bin (contours at the left hand side). The model spectra are composed of a ultraviolet-to-X-ray bump, characterized by a far UV power law and a cut-off energy, and of a power law spectrum at medium X-ray energies, the index of which is fixed to a previously determined value. The inset shows an enlargement of these contours. The right hand sided contours show the results of the same simulation, with an additional scaling, of the cutoff energy as predicted by thin accretion disk models ($\epsilon_{cut} \sim L^{-1/4}$).

 $\sum_{i=1}^{5} \left(\left(-1.5f_i + \Gamma_i (1-f_i) - < \Gamma_{obs} >_i \right) / \sigma (< \Gamma_{obs} >_i) \right)^2,$ where $< \Gamma_{obs} >_i$ and $\sigma (< \Gamma_{obs} >)_i$ are the means of the spectral slopes and their standard deviations determined for the different redshift bins *i*. In Table 10 the results are given for different fractions of f_i . They confirm the description given in the preceding section, namely that the soft X-ray excess determined from the data of the sample quasars is a lower limit. In particular, the cut-off energy derived from our observations for a given adhoc spectral shape of the ultraviolet-to-soft X-ray continuum

 $(f_i = 0)$ is a lower limit. These simulations show that, if the mean spectral shape of the soft X-ray excess does not vary with luminosity, the cut-off energy of the excess defined according to the two-component model given above is larger than 60 eV at a confidence level of 68.3% (45 eV at 90% confidence) (see inset of Fig.7). This lower limit of the cut-off energy for quasars compares very well with that obtained for Seyfert 1 galaxies (60 - 80 eV) by studying their ultraviolet and soft X-ray spectra (Walter et al., 1994). Furthermore, also the ratio between the ultraviolet and X-ray fluxes $\nu F_{\nu}(0.009 \text{ keV})/\nu F_{\nu}(2 \text{ keV}) = 13$, corresponding to a cut-off energy of 60 eV, matches very well the mean ratio observed for Seyfert 1 galaxies (Walter & Fink, 1993).

Kembhavi and Fabian (1994) have found that the range in cutoff energy permitted by the comparison of the optical quasar luminosity function with the soft X-ray quasar surface density is comprised between 50 and 150eV. This compares very well to the lower limit we derived from the redshift dependence of the mean quasar soft X-ray spectrum and suggests that selection effects are not affecting our data too much.

The cut-off energy of the soft X-ray excess is, therefore, similar in quasars and in Seyfert 1 galaxies. We can test our data for the predictions of thin accretion disk models with simulations which assume that the cut-off energy in the two-component model spectrum scales with $10^{-1/4(<\log L_{\rm opt_i})}/<\log L_{\rm opt_{i=1}}>)$ in the different redshift bins. This luminosity scaling was predicted by Shakura and Sunyaev (1973) and is still present in more advanced accretion disk models (e.g. Ross and Fabian, 1993). The contours at the lower right in Fig.7 show the result of this simulation for the free parameters $\epsilon_{cut}(L_{opt_{i=1}})$ and R. It indicates that the thin accretion disk model prediction is compatible with the redshift dependence of the soft X-ray spectrum only for a very restricted region of the parameter space, i.e. $\epsilon_{\rm cut} = 350^{+150}_{-100}$ eV and the flux ratio is $R = 0.32^{+0.19}_{-0.07}$.

This ratio R of the ultraviolet to X-ray fluxes is outside of the range permitted for Seyfert 1 galaxies (R = 1 - 100; Walter & Fink, 1993). For the nearby quasars in our sample we obtain in the first redshift bin an observed value of R > 3.2 also in contradiction to the value derived from the luminosity scaling of the thin accretion disk.

Furthermore, the cut-off energy determined is a lower limit as it will increase with steeper ultraviolet spectra as well as when the selection effects are taken into account. A lower limit of 250 eV predicted to be compatible with thin accretion disk models is three times larger than the upper limit found for individual sources observed simultaneously with IUE, ROSAT, and Ginga using the same model spectrum (Walter et al., 1994) and two times larger than the upper limit derived by Kembhavi and Fabian (1994). We also note that black body fits to the soft X-ray excesses observed with ROSAT yields temperatures very similar to the cut-off energies of the two-component model spectrum (Walter et al., 1994); the typical black body temperatures derived from ROSAT spectra of AGN are usually smaller than 100 eV. Larger temperatures are obtained by introducing hot absorbers onto the line of sight, but even in those cases the temperatures are limited to 150 eV (Pounds et al., 1994). We conclude therefore that our observations are not compatible with the luminosity dependence predicted by thin accretion disk models.

4.5. Radio-loud versus radio-quiet quasars

In previous sections we found for our sample that radio-loud as well as radio-quiet quasars exhibit appreciably steeper spectra at soft X-rays than in the medium energy range. This was interpreted as an indication for the existence of a flux excess at very soft photon energies in the soft X-ray spectra of both subclasses of quasars. Further it was stated that the indices of their spectra are significantly different from each other, if their soft X-ray emission is described by a simple power law.

Assuming that the quasar spectra in the ultraviolet to medium X-ray energy range can be represented by the two-component model described in Sect. 4.4.2 we firstly check what fraction of the mean soft X-ray component contributes to the flux in the ROSAT's energy band. Thereby, the photon indices of the medium energy power law component is fixed to $\Gamma_{\rm X}=1.5$ for radio-loud quasars and $\Gamma_{\rm X}=1.9$ for radio-quiet QSOs, respectively, whereas the power law spectrum of the soft component is set to $\Gamma_{\rm UV}=1.4$. The cut-off energy was chosen to be $\epsilon_{\rm cut}=60$ eV, the lower limit for the index-redshift relation of quasars. Defining the fraction F as

$$F = \left(\frac{F_{SE}}{F_{PL}}\right)_{0.1-2.4~keV} = \frac{A_2}{A_1} \cdot \frac{\int \left(\frac{E}{E_2}\right)^{-\Gamma_2} \cdot exp(\frac{E-E_2}{\varepsilon_{cut}})EdE}{\int \left(\frac{E}{E_1}\right)^{-\Gamma_1}EdE}$$

we have to establish a relation between F and the photon index Γ as resulting from simple power law parameter estimation of spectra simulated for a grid of weights (A_1,A_2) of the two spectral components. The method of simulation is similar to the

procedures described in Sect. 4.4.2 with A_2/A_1 as the free parameter. The resulting F- Γ calibration is obtained for radio-loud and radio-quiet mean spectra. Using this relation we transform the photon indices previously derived for the individual members of our sample into F values and determine the mean value for the subclasses. We restrict the study to objects with $z \le 0.5$, for which both subclasses are well populated and where a possible influence of the redshift is expected to be still small. We found that the mean fraction of the soft X-ray excess relative to the medium energy power law component is, within the limits of errors, the same in the (0.1 - 2.4)keV energy band for radio-loud as well as for radio-quiet quasars: $\langle F \rangle_{rl} = 0.70 \pm 0.08$ and $\langle F \rangle_{rq} = 0.69 \pm 0.05$. A similar result is obtained, if the cut-off energy is chosen to be 110 eV.

Taking the ratio of these measured mean F-values

$$(0.986 \pm 0.094) = \frac{\left(\frac{F_{SE}}{F_{PL}}\right)_{rl}}{\left(\frac{F_{SE}}{F_{PL}}\right)_{rq}} =$$

$$= \left(\frac{F_{rq}}{F_{rl}}\right)_{PL} = \left(\frac{A_{rq}}{A_{rl}}\right)_{PL} \cdot E_{PL}^{-0.4} \cdot \frac{\int E^{-1.9} E dE}{\int E^{-1.5} E dE}$$

we find for the same soft X-ray excess, i.e. $F_{SE_{rq}} = F_{SE_{rl}}$, that the medium energy power law components of radio-loud and radio-quiet quasar cross over at $E_{PL} \sim 0.6$ keV.

Assuming that the mean ultraviolet-to-soft X-ray bump has the same spectral shape in the spectra of radio-loud as well as of radio-quiet quasars, we, therefore, found that for the same mean excess component the medium energy power laws cross each other at a photon energy which is higher than that energy at which the excess component begins to dominate the soft X-ray spectrum ($\sim 0.3~{\rm keV}$). Beyond 0.6 keV the flux of the spectra of radio-loud quasars is much larger than the flux of radio-quiet QSOs for the same relative normalization at 0.6 keV. Furthermore, we found that the mean X-ray properties of the sample members can be described by a model spectrum which differs for both radio subclasses only in the mean spectral index of the hard X-ray component.

5. Summary and conclusions

The aim of the present study was the investigation of the overall properties of soft X-ray spectra of quasars observed during the ROSAT all-sky survey. The flux limited sample (≥ 80 SASS cts) selected by correlating X-ray point source survey positions with those of optically identified quasars contains 102 objects. The sample comprises 55 radio-quiet QSOs, whose redshifts range, with the exception of PG 1407+285 (z=0.94), from z=0 to z=0.5, and 47 radio-loud quasars with redshifts up to z=2.35. The low flux threshold does not allow to study the X-ray spectra of all sample quasars in detail. Therefore, a method was developed to estimate from hardness ratios simple spectral parameters like the spectral slope and the absorption column density of cold matter on the line of sight.

From these parameter estimations it could be shown that those X-ray bright AGN detected with ROSAT beyond the flux

50

threshold do not show strong intrinsic absorption; the low energy absorption in the soft X-ray quasar spectrum can be described by the Galactic column density in the source's direction. This lack of intrinsic absorption in our sample is certainly affected by a selection effect: sources with strong absorption would exhibit a deficit of photons in ROSAT's soft energy band, and, therefore, the photon flux of many of those sources would not meet the sample's limit.

Furthermore, we have to state that the power law indices of individual quasar spectra determined in ROSAT's (0.1 - 2.4)keV energy band are significantly higher than those well established indices at medium energies ≥ 2 keV known from previous measurements with the HEAO-1, Einstein, EXOSAT, and Ginga experiments. We confirm also for the soft energy band the previous finding that the slopes of power law spectra of radio-quiet and radio-loud quasars, respectively, are significantly different. Whereas a mean photon index of $<\Gamma>_{rq}=2.54\pm0.04$ was found for the members of the radio-quiet subclass, the mean index of the ROSAT spectra of radio-loud quasars was determined to be $<\Gamma>_{rl} = 2.23 \pm 0.07$.

In order to quantify the average difference between the soft X-ray slope and indices determined at higher photon energies, we compared the mean indices of identical subsamples of nearby quasars (z < 0.5) observed with ROSAT and with a medium energy experiment, respectively. A common quasar sample observed with ROSAT and with the Einstein Observatory (Wilkes & Elvis, 1987) comprises 25 objects. A comparison of the mean indices revealed that the IPC (0.3 - 3.5)keV indices are significantly smaller than the PSPC (0.1 - 2.4)keV indices: for radioquiet quasars (11 objects) the mean indices and the difference are $<\Gamma>_{(0.1-2.4)\text{keV}}=2.54\pm0.06, <\Gamma>_{(0.3-3.5)\text{keV}}=1.88\pm$ 0.12, $\Delta\Gamma = 0.66 \pm 0.14$, whereas for the radio-loud subgroup (14 objects) the corresponding values are $<\Gamma>_{(0.1-2.4)\text{keV}}=$ 2.20 ± 0.11 , $<\Gamma>_{(0.3-3.5)\text{keV}}=1.52\pm0.09$, $\Delta\Gamma=0.68\pm0.14$. Comparisons of identical quasar subsamples observed at photon energies larger than 2 keV with EXOSAT/ME (Lawson et al., 1992) and Ginga/LAC (Williams et al., 1992) confirm that the mean power law indices decrease with increasing hardness of the energy band for which the indices were determined.

The variety of radio-loud quasars in the ROSAT sample allows to study the slope of the mean spectrum as a function of redshift. By determining the mean indices in the (0.1 -2.4)keV energy band in the observer's frame for five redshift bins, an index-redshift relation is established. It shows a remarkable drop of the photon index from about $\Gamma = 2.2$ for quasars with redshifts z < 0.5 to $\Gamma = 1.5$ in the range z = 1.0 - 2.5, with a marked inflexion point at $z \approx 0.6$. It is noticeable that at high redshifts the mean soft index approaches the level of slope values measured at medium energies for nearby radio-loud quasars.

Although selection effects may account for some fraction of the observed flattening of the mean quasar spectrum with increasing redshift, the most plausible explanation of the redshift curve is a spectral steepening towards lower photon energies. Indeed, the redshift curve of the spectral steepness is well reproduced by adopting an ad hoc representation of the mean quasar spectrum consisting of a power law spectrum with a fixed index of $\Gamma_{UV} = 1.4$ and an exponentially cut-off at soft X-ray wavelengths superposed onto a medium energy power law spectrum with an index of $\Gamma_X = 1.5$. The best fit of this two-component model spectrum, which has proved to represent best the UV-to-X-ray spectra of Seyfert 1 galaxies (Walter et al., 1994), to the redshift curve yields a temperature $\epsilon_{cut} = 110 \ eV$. Taking the selection effects into account, a lower limit for this cut-off energy is $\epsilon_{cut} > 60 \, eV$ which agrees with the values measured for Seyfert 1 galaxies. We therefore conclude that the mean UV-to-X-ray spectrum of radio-loud quasars can be described by the same spectral shape as that of Seyfert 1 galaxies.

It has to be noted in particular that the data are not compatible with a cut-off energy increasing with luminosity as much as predicted by thin accretion disk models ($\epsilon_{cut} \sim L_{opt}^{-1/4}$). Thin accretion disk models are therefore not able to reproduce the spectral shape observed in Seyfert 1 galaxies and quasars without fine-tuning.

The comparison of radio-quiet and radio-loud quasars with z < 0.5 shows that the flux ratio of the excess component and the medium energy power law ($\Gamma_{rq} = 1.9$, $\Gamma_{rl} = 1.5$), extrapolated to ROSAT's energy band, is coincidently the same for both types of quasars when the mean quasar spectrum is represented by the two-component model mentioned above. Normalizing the spectra to the same mean excess we found that the medium energy power law spectra cross over at $E_o = 0.6 \text{ keV}$, - an energy which is beyond that soft X-ray energy where the excess component starts to rise, (~ 0.3 keV). Referring to the same strength of the excess component, the fact that the hard X-ray flux of radio-loud quasars beyond 0.6 keV is much larger than that of their radio-quiet counterparts does not support the idea that reprocessing of hard X-ray photons in cold, dense material produces the excess component. From our present study we can state that the mean spectra of radio-loud and radio-quiet quasars differ only in their medium energy power law indices. The excess components are indistiguishable.

Acknowledgements. The ROSAT mission is supported by the Ministerium für Forschung und Technologie, FRG, and by the Max-Planck-Society. We thank the SASS team for processing the all-sky survey data and the EXSAS team for providing a software package for the reduction of the ROSAT data. R.W. acknowledges a Max Planck Fellowship. This paper is part of a PhD thesis by N.S..

References

Angel J.R.P., Stockman H.S., 1980, ARA&A 18,321

Arnaud K.A., Branduardi-Raymont G., Culhane J.L., Fabian A.C., et al., 1985, MNRAS 217, 105

Aschenbach B., 1988, Apl. Optics 27, 1404

Bowyer C.S., Lampton M., Mack J., Mendonca F., 1970, ApJ 161, L1 Brinkmann W., Siebert J., 1994, A & A 285, 812

Brunner H., Friedrich P., Staubert R., et al., 1992, Soft X-ray spectra of radio-loud quasars: first results from the ROSAT survey. In: Duschl W.J., Wagner S.J. (eds.) Physics of Active Galactic Nuclei. Springer, Berlin, p.77

Canizares C.R., White J.L., 1989, ApJ 339, 27

Comastri A., Setti G., Zamorani G., Elvis M., et al., 1992, ApJ 348, 62

Della Ceca R., Zamorani G., Maccacaro T., et al., 1994, ApJ 430, 533 Dörrer T., Friedrich P., Brunner H. et al., 1992, MPE-Report 235, Brinkmann & Trümper (eds)

Elvis M., Wilkes B.J., Tananbaum H., 1985, ApJ 292, 357

Elvis M., Green R.F., Bechtold J., Schmidt M., et al., 1986, ApJ 310, 291

Elvis M., Lockman F.J., Wilkes B.J., 1989, AJ 97, 777

Elvis M., Fiore F., Mathur S., Wilkes B.J., 1994, ApJ 425, 102

Elvis M., Wilkes B.J., McDowell J.C., et al., 1994, ApJ Suppl. 95, 1 Fink H.H., Briel U.G., 1993, A&A 274, L45

Fiore F., Elvis M., McDowell J.C., Siemiginowska A., Wilkes B.J., 1994, ApJ 431, 515

Kellerman K.I., Sramek R., Schmidt M., Shaffer D.B., Green R., 1989, AJ 98, 1195

Kembhavi A., Fabian A.C., 1994, in "Multi-wavelength continuum emission of AGN", IAU-Symp 159, Courvoisier and Blecha (eds).

Kolman M., Halpern J.P., Shrader Ch.R., et al., 1993, ApJ 402, 514

Kruper J.S., Urry C.M., Canizares C.R., 1990, ApJS 74, 347

Kühr H., Nauber U., Paulini-Toth I.I.K., Witzel A., 1979, MPIfR preprint No.55

Laor A., Fiore F., Elvis M., Wilkes B.J., McDowell J.C., 1994, ApJ 435, 611

Lawson A.J., Turner M.J.L., Williams O.R., Stewart G.C., Saxton R.D., 1992, MNRAS 259, 743

Maccacaro T., Gioia I.M., Wolter A., Zamorani G., Stocke J.T., 1988, ApJ 326, 680

Matthews T.A., Sandage A. R., 1963, ApJ 138, 30

Mushotzky R., 1984, Adv. Space Res. 3, 157

Nandra K., Pounds K.A., 1994, MNRAS 268, 405

Nandra K., Fabian A.C., George I.M., et al., 1993, MNRAS 260, 504

Paltani S., Courvoisier T.J.-L., 1994, A&A 291, 74

Pounds K.A., Nandra K., Fink H.H., Makino F., 1994, MNRAS 267, 193

Predehl P., Schmitt J.H.M.M., 1994, A&A, in press

Ross R.R., Fabian A.C., 1993, MNRAS 261, 74

Saxton R.D., Turner M.J.L., Williams O.R., et al., 1993, MNRAS

Schmidt M., Green R.F., 1986, ApJ 305, 62

Schwartz D.A., Qian Y., Tucker W.H., 1989, Comparing measurements of AGN X-ray spectra with the shape of the diffuse X-ray background spectrum. In: Hunt J., Battrick B. (eds.) Proc. 23rd ESLAB Symp. on Two Topics in X-Ray Astronomy, Bologna, ESA SP-296, Vol.2, p.1043

Serlemitsos P., Yaqoob T., Ricker G., et al., 1994, NASA/LHEA preprint X-ray: 94-5

Shakura N.I., Sunyaev R.A., 1973, A&A 254, 22

Shastri P., Wilkes B.J., Elvis M., McDowell J., 1992, ApJ 410, 29

Singh K.P., Garmire G.P., Nousek J., 1985, ApJ 297, 633

Snowden S.L., Plucinski P.P., Briel U.G., Hasinger G., Pfeffermann E., 1992, ApJ 393, 819

Sramek R., Weedman D., 1980, ApJ 238, 435

Stark A.A., Gammie C.F., Wilson R.W., et al., 1992, ApJ Suppl. 79, 77

Trümper J., 1983, Adv. Space Res. 2, 241

Turner T.J., Pounds K.A., 1989, MNRAS 240, 833

Ulrich M.-H., Fink H.H., Schaeidt S., et al., 1992, A&A 266, 183

Véron-Cetty M.-P., Véron P., 1991, A catalogue of quasars and active nuclei (5th Edition). ESO Scientific Report No.10

Voges W.,1992, The ROSAT all-sky X-ray survey. In: Guyenne T.D., Hunt J.J. (eds.) European International Space Year Conference 1992, Space Science. ESA ISY-3, p.9

Voges W., Gruber R., Paul J., et al., 1992, The ROSAT standard analysis software system. In: Guyenne T.D., Hunt J.J. (eds.) European

International Space Year Conference 1992, Space Science. ESA ISY-3, p.223

Walter R., Fink H.H., 1993, A&A 274, 105

Walter R., Orr A., Courvoisier T.J.-L., et al., 1994, A&A 285, 119

Wilkes B.J., Elvis M., 1987, ApJ 323, 243

Wilkes B.J., Elvis M., Fiore F., et al., 1992a, ApJ 393, L1

Wilkes B.J., Elvis M., Fiore, F., McDowell, J.: 1992b Havard-Smithsonian Center for Astrophysics, preprint No.3514

Williams O.R., Turner M.J.L., Stewart G.C., et al., 1992, ApJ 389, 157Wills B.J., Wills D., Breger M., Antonucci R.R.J., Barvainis R., 1992, ApJ 398, 454

Worrall D.M., 1989, Population properties of AGN in the soft X-ray band. In: Hunt, J., Battrick, B. (eds.) Proc. 23rd ESLAB Symp.on two topics in X-ray Astronomy. ESA SP-296, p.719

Yaqoob T., Serlemitsos P., Mushotzky R., et al., 1994, PASJ 46,L43 Zamorani G., Henry J.P., Maccacaro T., et al., 1981, ApJ 245, 357

This article was processed by the author using Springer-Verlag LATeX A&A style file version 3.